95

①

AD-A218 325

The Pennsylvania State University

The Graduate School

A CASE STUDY OF A QUASI-STATIONARY TROPICAL CONVECTIVE LINE

A Thesis in

Meteorology

by

Jeffrey Lynn Peters

Submitted in Partial Fulfillment
of the Requirements
for the Degree of

Master of Science

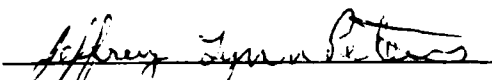August 1989

90 02 21 095

I grant The Pennsylvania State University the nonexclusive right to use this work for the University's own purposes and to make single copies of the work available to the public on a not-for-profit basis if copies are not otherwise available.

_____

Jeffrey Lynn Peters

REPORT DOCUMENTATION PAGE		Form Approved OMB No. 0704-0188
1a. REPORT SECURITY CLASSIFICATION UNCLASSIFIED	1b. RESTRICTIVE MARKINGS NONE	
2a. SECURITY CLASSIFICATION AUTHORITY	3. DISTRIBUTION/AVAILABILITY OF REPORT APPROVED FOR PUBLIC RELEASE; DISTRIBUTION UNLIMITED.	
2b. DECLASSIFICATION/DOWNGRADING SCHEDULE		
4. PERFORMING ORGANIZATION REPORT NUMBER(S)	5. MONITORING ORGANIZATION REPORT NUMBER(S) AFIT/CI/CIA- 89-075	

6a. NAME OF PERFORMING ORGANIZATION AFIT STUDENT AT PENN STATE UNIVERSITY	6b. OFFICE SYMBOL (If applicable)	7a. NAME OF MONITORING ORGANIZATION AFIT/CIA
6c. ADDRESS (City, State, and ZIP Code)		7b. ADDRESS (City, State, and ZIP Code) Wright-Patterson AFB OH 45433-6583
8a. NAME OF FUNDING/SPONSORING ORGANIZATION	8b. OFFICE SYMBOL (If applicable)	9. PROCUREMENT INSTRUMENT IDENTIFICATION NUMBER

8c. ADDRESS (City, State, and ZIP Code)	10. SOURCE OF FUNDING NUMBERS			
	PROGRAM ELEMENT NO.	PROJECT NO.	TASK NO	WORK UNIT ACCESSION NO.

11. TITLE (Include Security Classification) (UNCLASSIFIED)
A Case Study of a Quasi-Stationary Tropical Convective Line

12. PERSONAL AUTHOR(S)
Jeffrey Lynn Peters

13a. TYPE OF REPORT THESIS/DISSERTATION	13b. TIME COVERED FROM_____ TO_____	14. DATE OF REPORT (Year, Month, Day) 1989 August	15. PAGE COUNT 84

16. SUPPLEMENTARY NOTATION
APPROVED FOR PUBLIC RELEASE IAW AFR 190-1
ERNEST A. HAYGOOD, 1st Lt, USAF
Executive Officer, Civilian Institution Programs

17.	COSATI CODES		18. SUBJECT TERMS (Continue on reverse if necessary and identify by block number)
FIELD	GROUP	SUB-GROUP	

19. ABSTRACT (Continue on reverse if necessary and identify by block number)

20. DISTRIBUTION/AVAILABILITY OF ABSTRACT ☒ UNCLASSIFIED/UNLIMITED ☐ SAME AS RPT. ☐ DTIC USERS	21. ABSTRACT SECURITY CLASSIFICATION UNCLASSIFIED	
22a. NAME OF RESPONSIBLE INDIVIDUAL ERNEST A. HAYGOOD, 1st Lt, USAF	22b. TELEPHONE (Include Area Code) (513) 255-2259	22c. OFFICE SYMBOL AFIT/CI

DD Form 1473, JUN 86   *Previous editions are obsolete.*   SECURITY CLASSIFICATION OF THIS PAGE

AFIT/CI "OVERPRINT"

We approve the thesis of Jeffrey Lynn Peters.

Date of Signature

[signature]

George S. Young
Assistant Professor of Meteorology
Thesis Adviser

April 7 1989

[signature]

Bruce A. Albrecht
Associate Professor of Meteorology

April 7 1989

[signature]

William M. Frank
Professor of Meteorology
Head of the Department of Meteorology

10 April 1989

ABSTRACT

An extreme case of a convectively dominated tropical convective system was investigated. Of particular interest is the observation that the nimbostratus anvil (produced by the convective line was an order of magnitude smaller than most of the nimbostratus anvils) observed during GATE. Flight level data from the NCAR Electra was composited to examine the thermodynamic and kinematic structure of the convective line, of the environment, and of the wake. The boundary layer structure was studied using bulk aerodynamic surface fluxes and eddy correlation turbulence statistics.

The review of the environmental thermodynamics showed that these factors did not control the velocity of the convective line or the production of nimbostratus anvil. The study of the kinematic structure and a review of previous studies determined that the ability of a convective line to produce nimbostratus anvil is a function of horizontal moisture advection from the convective region into the mesoscale stratiform anvil region. The advection of moisture into the mesoscale stratiform anvil region is controlled both directly and indirectly via across line shear and line speed.

The bulk aerodynamic surface fluxes gave a wake recovery time on the order of 10 hours, and eddy correlation turbulence statistics were found to provide insight into the boundary layer forcing and turbulence structure.

TABLE OF CONTENTS

TABLE OF CONTENTS (continued)

LIST OF TABLES

LIST OF FIGURES

LIST OF FIGURES (continued)

ACKNOWLEDGEMENTS

Chapter 1

INTRODUCTION

A tropical convective line is a mesoscale linear array of active cumulonimbus clouds (convective cells). The initial convective cells usually form along a discontinuity in the boundary layer thermodynamic field or in an area of enhanced boundary layer convergence. Subsequent convective cells often develop on the gust front associated with the cold downdraft air from these cells. The convective line contributes to an associated stratiform precipitation area by feeding moisture into the mid and upper troposphere. Tropical convective lines have been compared to mid-latitude squall lines and share many of the same characteristics.

Convective lines have been studied since Hamilton and Archbold (1945) examined their structure in Nigeria. Many case studies and numerical simulations of convective lines have followed. Researchers have spanned the globe in studying these lines. Zipser (1977) examined the mesoscale and convective-scale downdrafts of convective lines over Barbados. Betts et al. (1976) studied the structure of tropical convective lines over Venezuela. Mid-latitude convective lines in Kansas and Oklahoma have been researched by Newton (1950), Fujita (1955), Pedgley (1962), Ogura and Liou (1980), Smull and Houze (1985), and others.

The Global Atmospheric Research Programs' Atlantic Tropical Experiment (GATE), conducted in 1974 over the waters west of equatorial Africa, was the first experiment to provide comprehensive data for the study of the structure and life cycle of tropical convective lines. COPT 81 (Convection Profonde Tropicale), conducted in the Ivory Coast, added to the data available for the study of tropical convective lines. The most recent experiment which collected data on tropical convective lines was EMEX (Equatorial Mesoscale Experiment) which was conducted over the waters north of Australia.

1.1 Objectives and Motivation

A primary reason for the comprehensive study of tropical convective lines is to improve our understanding of how they influence the general circulation in the tropics. (e.g. the Hadley and Walker cells). It is generally accepted that the existence or non-existence of tropical convective lines and their associated mesoscale stratiform anvils usually is the cause of large scale thermodynamic forcing (diabatic heating/cooling) changes in the tropics (Hartmann et al.,1984). This forcing includes latent heat release in the convective and stratiform components of convective lines as well as the related surface fluxes of latent and sensible heat.

Johnson and Young (1983) studied the heat budgets of a tropical cloud cluster (an area of clouds created by the interaction of multiple cumulonimbus and convective lines) and noted the maximum diabatic heating in the mesoscale stratiform anvil occurred near 350 mb. In the lower troposphere, a diabatic cooling maximum was found near 700 mb caused by evaporation and melting. Houze (1982) calculated the diabatic heating for isolated convective towers and found a much deeper positive in the heating profile with maximum diabatic heating near 550 mb. Thus, a convective line without a mesoscale stratiform anvil appears to have a much different diabatic heating profile than a mesoscale stratiform anvil producing convective line. Hartmann et al. (1984) examined the influence of different heating profiles on the Walker circulation using a linear model. They compared results from models run with a convective tower heating profile and with a heating profile characteristic of a mesoscale anvil producing tropical cloud cluster. The simulations were more realistic when the heating profile of a tropical cloud cluster was used. This suggests that the large scale wind fields may be sensitive to diabatic heating profile changes caused by variations in the relative contribution of convective and stratiform precipitation to the total.

The modification of the boundary layer by a convective line results in differences in the surface fluxes of sensible and latent heat between the pre-storm environment and the wake region.

Johnson and Nicholls (1983) calculated the surface sensible heat flux to be a factor of 5 greater in the wake region under the anvil at a distance approximately 100 km behind the leading edge of the convective line than in the undisturbed boundary layer ahead of the convective line. The increased surface flux in the wake region was a result of increased surface winds and reduced air temperatures. Johnson and Nicholls (1983) also calculated the surface latent heat flux difference between the undisturbed environmental boundary layer and the wake region. The results were similar to those for sensible heat flux with the surface latent heat flux in the wake region approximately 200% greater than in the undisturbed environment. The increase of surface latent heat flux in the wake region was attributed to surface drying and stronger winds in this region. Similar flux changes were also found by Garstang (1967) over the Atlantic. The enhanced fluxes in the wake regions of convective lines increase the total fluxes in the tropics over what would be expected in a purely undisturbed regime. Averaged over the tropics, this increase in surface fluxes in disturbed areas will support a corresponding increase in precipitation and, thus, in diabatic heating. Therefore, the thermodynamic characteristics of the wake region ultimately affects the general circulation in the tropics.

The goal of the current study is to provide key elements of the meteorological information needed to parameterize these critically important diabatic affects of convection in general circulation models. A tropical convective line that was observed to have a very limited area of nimbostratus anvil will be discussed. Because the region of nimbostratus anvil was far less extensive than with a typical convective line, the diabatic heating profile is expected to be dominated by the convective component as assumed for the conventional diabatic heating profiles studied by Hartmann et al. (1984). The surface fluxes in the wake region may also be influenced by the extent of the nimbostratus anvil region. In order to correctly parameterize the effect of convection in general circulation models, the diabatic heating profile and the surface fluxes of sensible and latent heat must be correctly related to characteristics of the large scale environment.

Therefore, it is quite important to determine from the large scale environmental conditions the extent of nimbostratus anvil produced by the parameterized convective lines. To determine why the convective line in the current study produced very little nimbostratus anvil, a detailed analysis of the thermodynamic and kinematic structure of the convective line and of its environment will be accomplished.

1.2   The Structure and Environment of Fast and Slow Convective Lines

The thermodynamic and kinematic structure of the convective line and its environment has been investigated by Houze (1977), Barnes and Sieckman (1984), Roux et al. (1984), Szoke and Zipser (1986), Smull and Houze (1987), Hauser et al. (1988), and others. The convective lines have been organized into three classes with the distinguishing characteristic being their speed (v) relative to the earth. The three classes are fast-moving $(v > 7\ ms^{-1})$, intermediate-moving $(3\ ms^{-1} \leq v \leq 7\ ms^{-1})$ and slow-moving $(v < 3\ ms^{-1})$. Barnes and Sieckman's (1984) suggestion that the type of convective line to form may be affected by the initial thermodynamic and kinematic environmental conditions offers the possibility of parameterizing the line type in a general circulation model.

Figure 1 (Houze, 1977) is a cross section through a convective line. These systems are composed of a convective region, a transition region, and a mesoscale stratiform anvil region. The convective region consists of cumulonimbi as defined by Byers and Braham (1949). The updrafts in mature cells are typically 0.9 km in diameter (LeMone and Zipser, 1980). The mature cells reach heights of 16-17 km with updrafts and downdrafts magnitudes on the order of 1-10 ms^{-1}. The typical width of the convective region is 20-40 km and the typical length is 150-300 km.

The updrafts of the cumulonimbus feed off the environmental boundary layer air ahead of the system. When the downdrafts form, a gust front is formed from the dense downdraft air. The
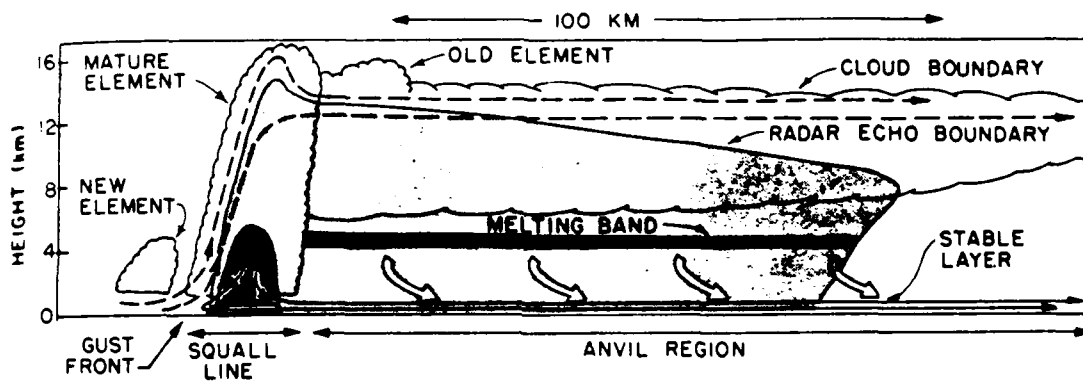
Figure 1: Schematic cross section through a squall-line system, from Houze (1977).

downdraft air spreads out along the surface and enhances convergence in the boundary layer in advance of the convective line triggering new convection. As new cumulonimbus form on the gust front, the mature cells begin to decay. Eventually the decaying cells are left behind by the progression of the gust front and associated new convection, and they are advected into the transition zone. The transition region is characterized by weaker radar reflectivities with little precipitation and ragged cumulonimbus remnants. The width of the transition region is approximately 20 km.

The mesoscale stratiform anvil region is the most extensive region of the convective line system, frequently extending behind the convective line some 50-500 km. The mesoscale stratiform anvil is formed from the merging upper level outflows from active cumulonimbus cells and cumulonimbus debris from the transition region. This anvil is composed of two components, non-precipitating cirrostratus in the upper troposphere and precipitating nimbostratus with bases near the melting level. The precipitation from the nimbostratus region can account for up to 40% of the total rain from a convective line (Houze, 1977). Houze (1977) concluded that the amount of rainfall from the nimbostratus anvil was greater than would be expected if the nimbostratus anvil was composed solely of inactive debris advected off the tops of the cumulonimbus making up the convective line. The existence of mesoscale updrafts within the nimbostratus anvil was postulated to explain this discrepancy. Gamache and Houze (1982) confirmed the existence of a mesoscale updraft overlaying a mesoscale downdraft in the transition and mesoscale stratiform anvil regions by using composited vertical velocities. This mesoscale updraft and the mid-level inflow which feeds it are responsible for the extra precipitation. The nimbostratus anvil is also characterized by a radar bright band that appears near the melting level. Zipser (1969) hypothesized that the cooling caused by melting and evaporation within the bright band is responsible for the observed mesoscale downdraft.

Barnes and Sieckman (1984) composited rawinsonde data from GATE to compare the environments of fast-moving and slow-moving convective lines. They found that fast-moving lines are characterized by vertical shear of the horizontal wind which is normal to the leading edge, while slow-moving lines have vertical shear of the horizontal wind which is parallel to the leading edge. Table 1 shows selected thermodynamic and kinematic parameters of the composited GATE soundings done by Barnes and Sieckman (1984). These observations show the thermodynamic structure of the environment to be quite similar for the fast-moving and slow-moving lines.

Using the means in the lowest 50 mb, Barnes and Sieckman (1984) showed the environmental equivalent potential temperature for a fast-moving line was 347.9 K while it was 348.5 K for a slow-moving line. The Lifted Index (T_{500} - T_{parcel}) was shown to be nearly identical, but the net convective available potential energy (CAPE, the positive area of a sounding) was found to be greater for the slow-moving line. Because the environmental thermodynamics of these two types of GATE convective lines were so similar, it can be concluded that environmental thermodynamic factors did not control the velocity of GATE convective lines. These observations do not support the modeling results of Moncrieff and Miller (1976) who concluded that the propagation speed of cumulonimbi and convective lines was determined by the CAPE and the mid level wind speed.

Figure 2 shows the vertical profile of the velocity components normal and tangential to the leading edge of the composite fast-moving line. Figure 3 presents the corresponding information for the composite slow-moving line. The storm relative normal velocity (v_n-v) for the environment of a fast-moving line has a maximum in the boundary layer and becomes negative (easterly) from approximately 3000 m to 4400 m. Above 4400 m, which is a relatively dry region and is near the freezing level, the storm relative normal velocity for the fast moving line's environment becomes positive (westerly) which is significant for the advection of moisture into the mesoscale stratiform anvil region. Figure 3 shows that the storm relative normal velocity for the environment of the composite slow-moving line is significantly less in the boundary layer and

Table 1: Thermodynamic and kinematic parameters of GATE composite soundings, from Barnes and Sieckman, 1984.

Parameter	Fast-moving Environment	Wake	Slow-moving Environment	Wake
Means in first 50 mb:				
Mixing ratio (gkg^{-1})	7.1	15.0	16.9	16.5
θ (K)	298.1	297.3	298.7	298.0
θ_e (K)	347.9	341.2	348.5	346.3
LCL (mb)	962	973	952	971
LFC (mb)	960	808	938	925
CAPE ($kJkg^{-1}$):				
LCL → LFC	0.001	-0.078	-0.004	-0.012
LFC → EL	1.004	0.146	1.230	0.422
Net CAPE	1.003	0.068	1.226	0.410
v_n (ms^{-1})	12		0.5	
v_t (ms^{-1})	< 0.5		6.2	
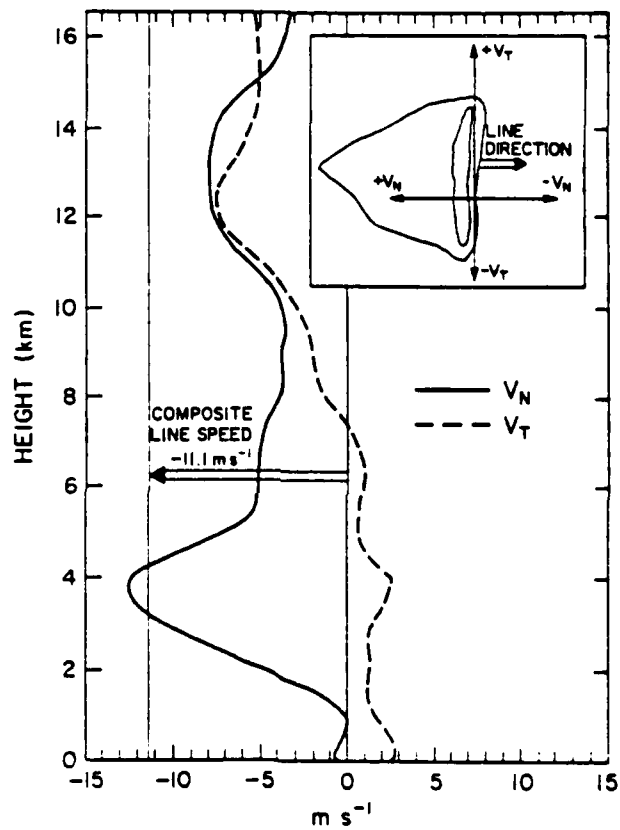
Figure 2: Composite profile of v_n and v_t to the leading edge of a fast-moving GATE convective line, from Barnes and Sieckman (1984).
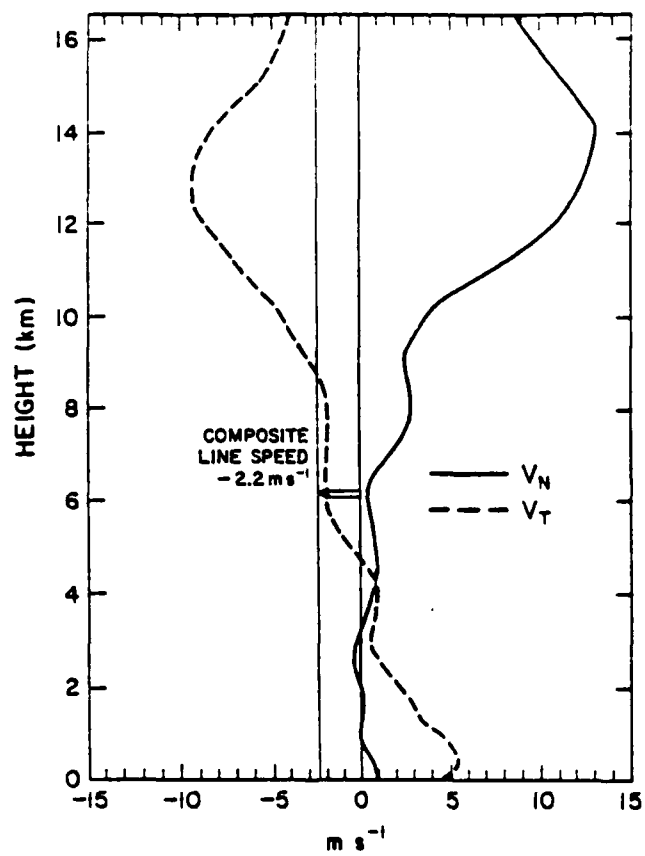
Figure 3:   Composite profile of v_n and v_t to the leading edge of a slow-moving GATE
convective line, from Barnes and Sieckman (1984).

between 4800 m to 7500 m compared with the environment of the composite fast-moving line. Barnes and Sieckman (1984) suggested that the mesoscale stratiform anvil regions associated with slow-moving lines are less extensive than with fast-moving lines. Modeling results by Cohen and Frank (1987) suggest that the nimbostratus anvil forms primarily from air originating in cumulus updrafts. The advection of decaying cumulonimbus by the line relative normal velocity may have an impact on the production of nimbostratus anvil. Houze (1977) hypothesized that the nimbostratus anvil evolved in part by the advection of a deep layer of convective line debris. Thus, the contribution of the diabatic heating profile of the anvil region to the total profile for the convective line may be controlled to a large degree by the environmental wind profile.

1.3 Boundary Layer Structure of Environment and Wake

Knowledge of the boundary layer structure of the pre-storm environment and post-storm wake region is vital when trying to determine the influence of convective lines on surface fluxes. The environment is the undisturbed convective boundary air ahead of the leading edge, while the wake is the boundary layer air behind the convective line which was altered by the convection. The boundary layer air in the wake has its origins in convective downdrafts. This air spreads out behind the convective line and can extend to 500 km behind the line. The nature and extent of these wakes have been studied by several authors.

Barnes and Sieckman (1984) and Johnson and Nicholls (1983) found substantial differences in the thermodynamic structure of the boundary layer between the environment and the wake. Figure 4 shows a large difference in the depth of the mixed layers between the environment and the wake regions. Johnson and Nicholls (1983) found a shallow mixed layer that started approximately 100 km behind the leading edge of the convective line. They also showed that from the gust front to 100 km behind the leading edge the mixed layer was less than 50 m deep if
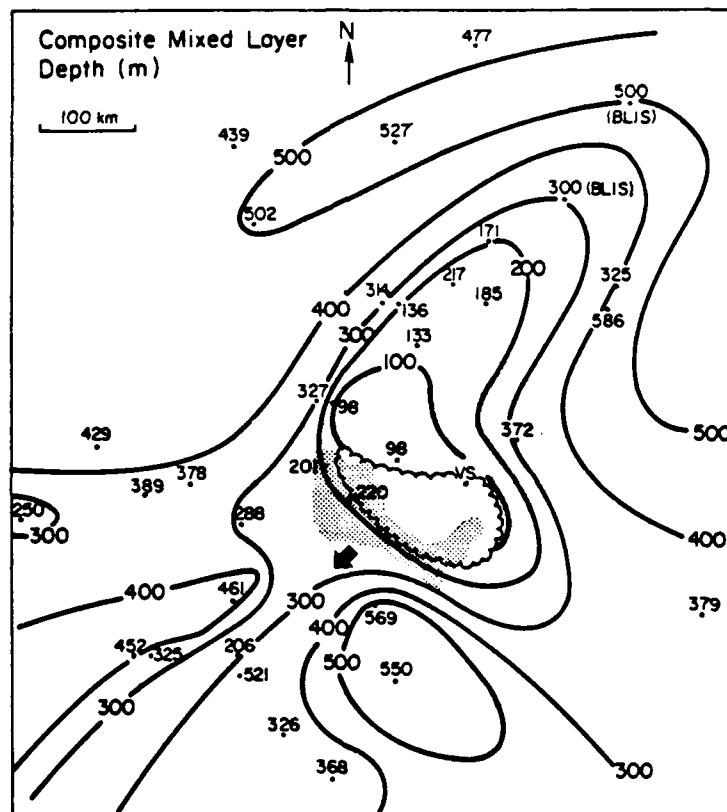
Figure 4: Composited mixed layer depth (m) for a GATE fast-moving line, from Johnson and Nicholls (1983).

present at all. Behind the leading edge, Johnson and Nicholls (1983) found large increases in surface fluxes of latent and sensible heat which would contribute significantly to the recovery of the mixed layer. On the north side of the wake, the mixed layer did not recover to its pre-storm depth until approximately 500 km behind the leading edge. On the south side of the wake, the mixed layer was recovered at approximately 300 km behind the leading edge. Johnson and Nicholls (1983) attributed this difference to mesoscale asymmetries in the composited flow field in the wake region and/or to the intensity of the convection associated with the convective line. In general, Johnson and Nicholls (1983) concluded that the strength of the subsidence or the mesoscale downdraft likely affected the recovery of the mixed layer with strong subsidence leading to slower wake recovery. Krueger (1988) presented modeling results that supported the large increase in the surface fluxes of sensible and latent heat in the wake. Barnes and Sieckman (1984) found significant differences in the line induced boundary layer changes of temperature and equivalent potential temperature between fast-moving and slow-moving lines. They found 1-2 K cooler boundary layer temperatures in the wake region compared to the environment of a slow-moving line, whereas 4-7 K cooler boundary layer temperatures were found in the wake region compared to the environment of a fast-moving line. The equivalent potential temperature drop between pre-storm environments and wake regions was also much greater for fast-moving lines, 6.7 K compared with 2.2 K.

Barnes and Sieckman (1984) showed that the change in stability between the environment and the wake region for the composited fast-moving and slow-moving convective line was also distinctly different. The net convective available potential energy in the wake region of a fast-moving line was 6.8% of the environment value, while the net CAPE in the wake region of a slow-moving line was 33.5% of the environmental value.

This modification of the convective boundary layer can hinder the formation of subsequent convection over the disturbed area. Thus, the rate of recovery of the disturbed region through

surface fluxes of sensible and latent heat becomes vital to the formation of new convection in the disturbed region.

1.4   The EMEX Experiment: Procedures and Data

EMEX (Equatorial Mesoscale Experiment) was conducted in January and February of 1987 over the waters north of Australia. The main objective of EMEX was to test the hypothesis that the diabatic heating associated with mesoscale convective systems (convective lines and cloud clusters) is strongest in the upper troposphere (Gamache et al., 1987). For this hypothesis to be valid, the stratiform precipitation region associated with these systems must contribute significantly to the overall diabatic heating.

The current study focuses on a quasi-stationary convective line over the Gulf of Carpentaria which was probed during the second EMEX aircraft mission (15 January 1987). The structure of the EMEX 2 convective line was examined using 1 Hz and 20 Hz aircraft flight level data from the NCAR Electra and NOAA P-3 aircraft, as well as Doppler and conventional radar data from the NOAA P-3 aircraft. The mesoscale environment in which the convective line persisted was studied using flight level data from the NCAR Electra, NOAA P-3, and CSIRO Fokker aircraft, as well as Omega dropwinsonde data from the NOAA P-3 aircraft and rawinsonde ascents from surrounding coastal stations.

The EMEX 2 convective line displayed many of the characteristics of the GATE convective lines studied by Frank (1978), LeMone and Zipser (1980), Johnson and Nicholls (1983), Barnes and Sieckman (1984), and Szoke and Zipser (1986). However, the nimbostratus anvil of the EMEX 2 convective line was approximately an order of magnitude smaller than the nimbostratus anvils commonly observed during GATE and in other EMEX system. Thus, EMEX 2 is an extreme case of a convectively dominated systems. This is shown in figure 5.
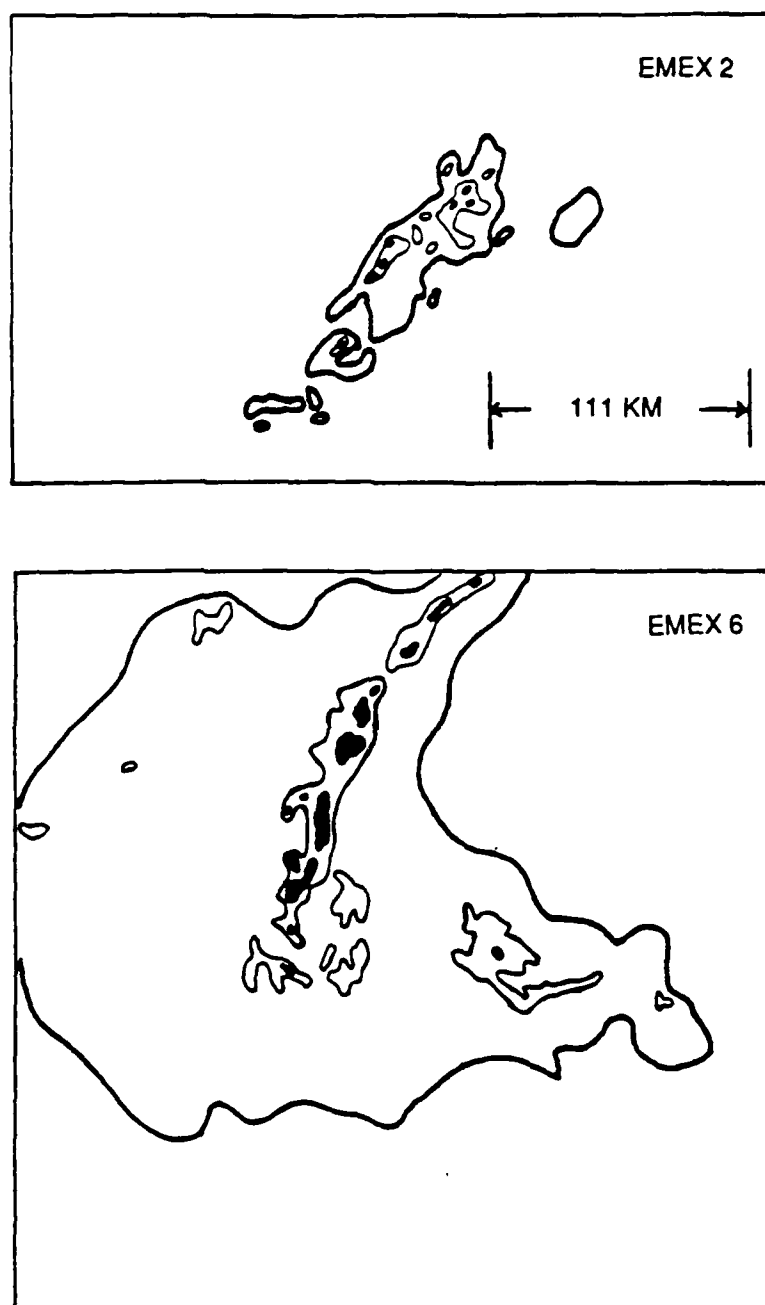
Figure 5: Comparison of horizontal extent of the EMEX 2 system with that of the EMEX 6 system.

Chapter 2

STORM HISTORY AND STRUCTURE DETERMINED FROM RADAR OBSERVATIONS

The radar data from the NOAA P-3 aircraft allows for a unique view of the history and structure of the EMEX 2 convective lines. In this chapter radar data are used to estimate line propagation and to provide insight on line and cell structure.

2.1 Storm History

In chapter 1, the convective line classification scheme of Barnes and Sieckman (1984) was discussed. This section will discuss if the EMEX 2 convective line can be placed within the Barnes and Sieckman (1984) classification scheme. To this end, isochrone analysis and several PPI scans will be reviewed to determine line speed.

2.1.1 Isochrone Analysis

Figure 6 shows the isochrones of the northwest edge of the radar echoes from the convective lines of 15 January 1987. At 1931 GMT, there was an extensive area of old stratiform precipitation to the southeast, and line 1 had already formed. From the AMEX radar atlas (Keenan and Martin, 1987), it is clear that the old stratiform region resulted from a convective line that dissipated before the EMEX 2 flight legs began. From 1931 GMT to 2110 GMT, line 1 continued to develop and new cells formed to the northwest of the line. The old stratiform region dissipated during this time and was entirely gone by 2110 GMT. The period between 2110 GMT and 2247 GMT brought great change to the structure of line 1, and line 2 formed during this period. Line 1 started to dissipate at 2232 GMT, and line 2 started to form at 2125 GMT. Line 1
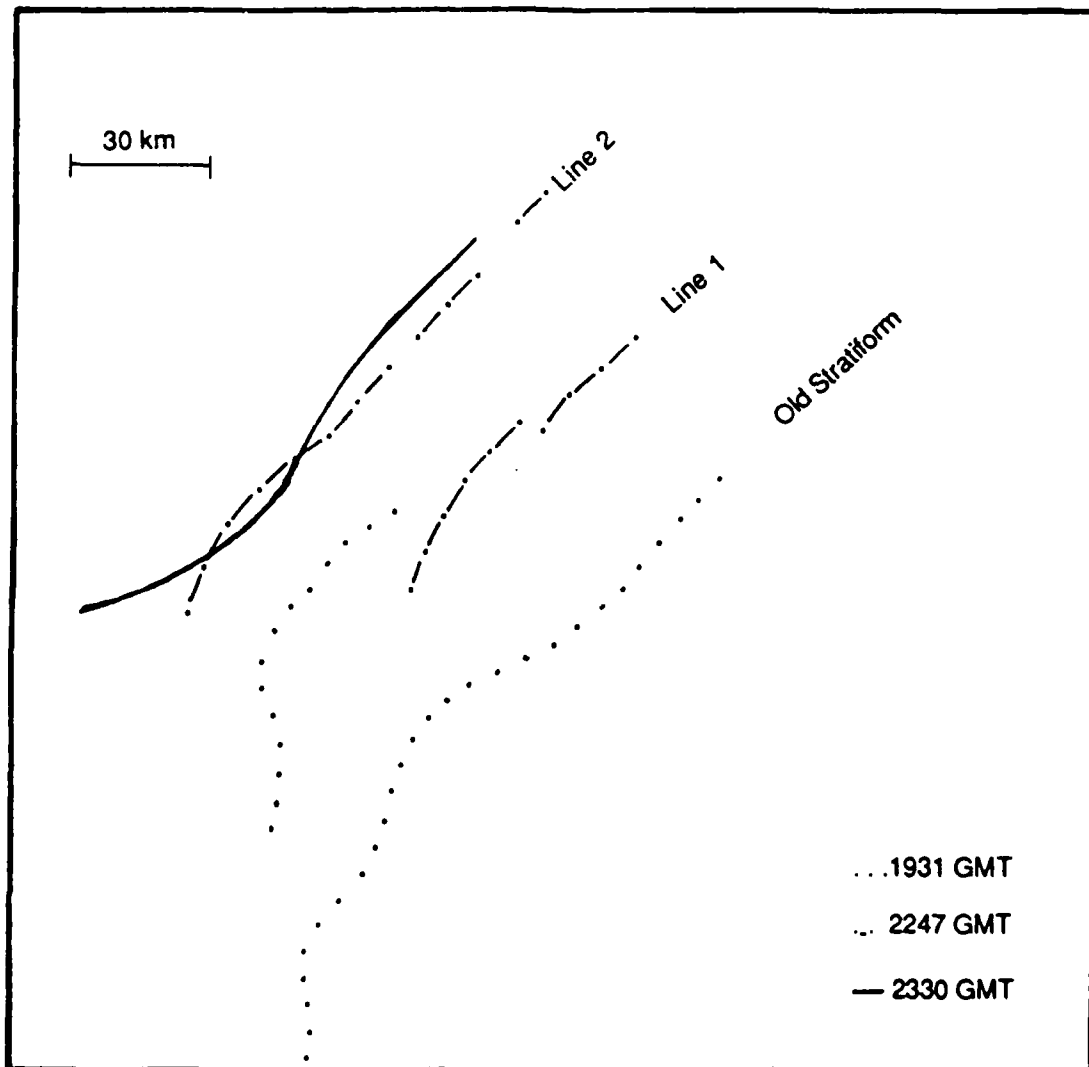
Figure 6:   Isochrones of the northwest edge of radar echoes.

still existed at 2247 GMT, but the northwest edge of the line showed no forward propagation; also line 2 was mature by 2247 GMT. By 2330 GMT, line 1 had fully dissipated. Thus, line 2 was the only existing line, and its northwest edge had propagated slightly to the northwest. The speed of line 2 was calculated to be 0.5 ms^{-1} with a possible error of ±0.5 ms^{-1}.

2.1.2 PPI Display

The PPI display from the NOAA P-3 aircraft provides a good depiction of the horizontal structure of the precipitation areas of 15 January 1987. Figures 7 to 10 are a series of PPI scans reviewing the history of the old stratiform region to the southeast, of line 1, and of line 2. Figure 7 shows that line 1 had formed approximately 30 km to the northwest of the old stratiform region. By 2020 GMT, the stratiform region (fig. 8) has virtually dissipated, and line 1 remains the only existing convective line. At this time line 1 is in the intensifying stage (Leary and Houze, 1979). Line 2 formed at approximately 2125 GMT roughly 33 km to the northwest of the leading edge of line 1. Figure 9 shows that line 1 had progressed into the mature stage (Leary and Houze, 1979). However, it had not started to produce the nimbostratus anvil which is a characteristic of the mature stage. Line 1 continued to dissipate and by 2330 GMT it was barely detectable (fig. 10). Throughout the mature and dissipating stage, line 1 never produced the nimbostratus anvil characteristic of previously studied tropical convective lines. Line 2 became mature by 2247 GMT. Line 2 also failed to produce a nimbostratus anvil throughout its mature stage.

A review of PPI scans including the 4 shown indicated that there was discrete propagation occurring with an approximately 35 km gap between successive lines. Despite the propagation of the entire EMEX 2 system, convective lines 1 and 2 remained virtually stationary. These two convective lines did not produce the nimbostratus anvil characteristic of most previously studied tropical convective lines.
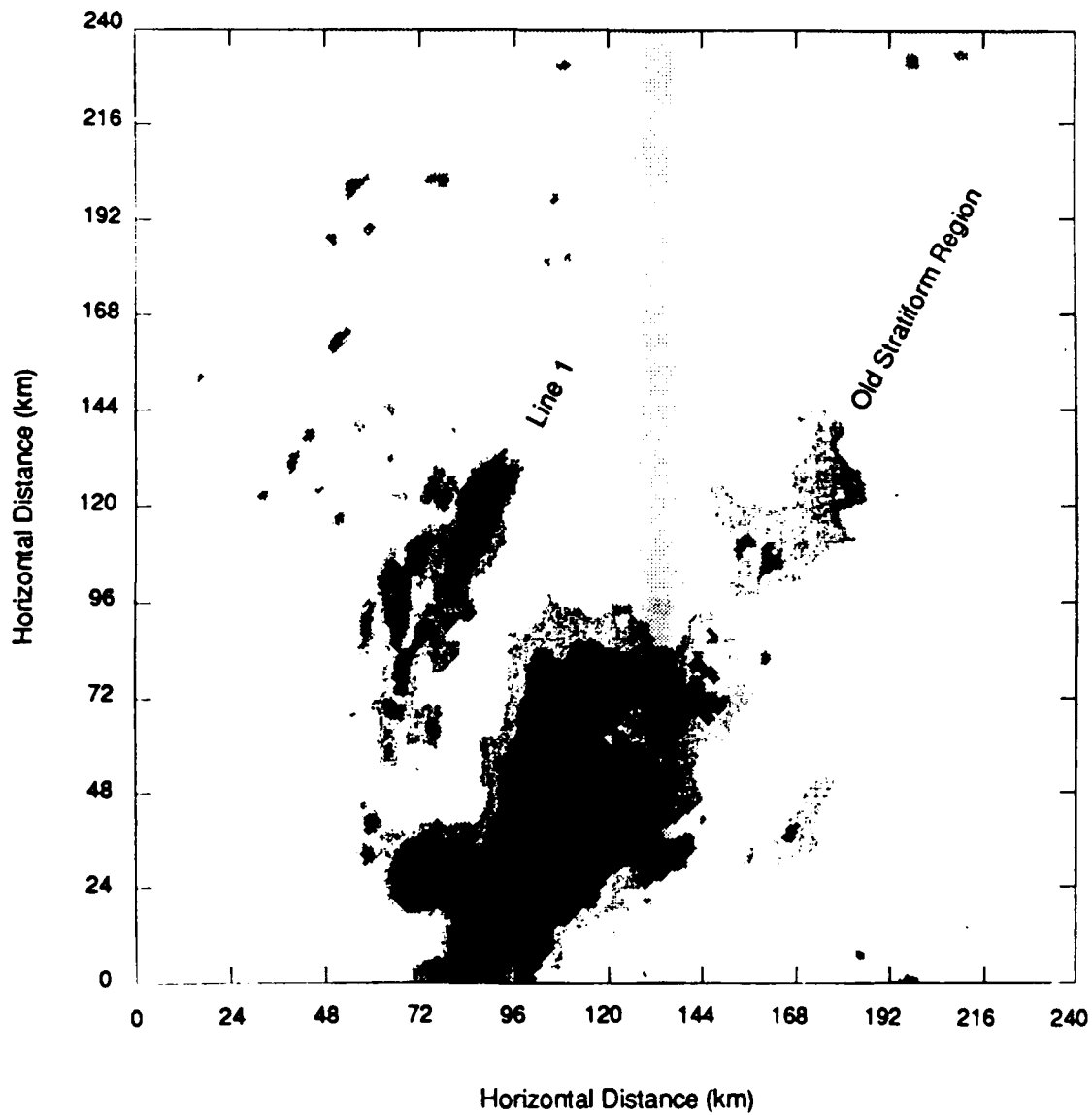
Figure 7:   PPI scan of line 1 and old stratiform region at 1931 GMT. Contours are for 11, 17, 24, 33 dBZ.
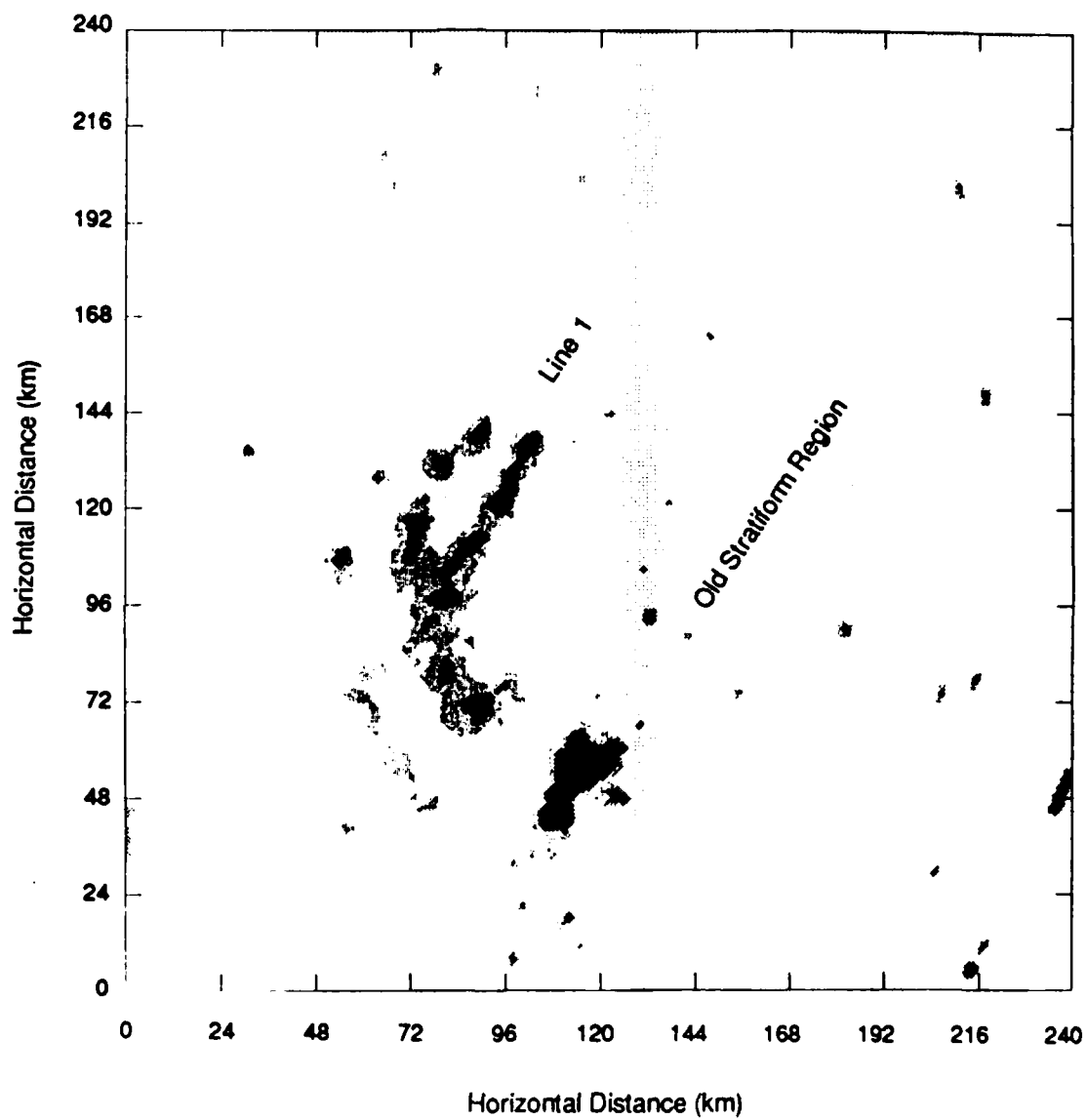
Figure 8:   PPI scan of line 1 and the remains of the old stratiform region at 2020 GMT. Contours are for 11, 17, 24, 33 dBZ.

Figure 9: PPI scan of lines 1 and 2 at 2155 GMT. Contours are for 11, 17, 24, 33 dBZ.

Figure 10: PPI scan of lines 1 and 2 at 2330 GMT. Contour are for 11, 17, 24, 33 dBZ.

2.2   Storm Structure Determined from Radar Observations

Storm structure of the EMEX 2 convective lines will be examined and compared to the stages presented in figure 11 from Leary and Houze (1979). RHI scans from the NOAA P-3 aircraft will be used to examine the vertical structure.

The convection that occurred on 15 January 1987 was vigorous as indicated by the depth and reflectivity of the cell shown in figure 12. This cell is associated with line 2 and is typical of the well developed, mature, cells that existed along lines 1 and 2. Some of these cells reached a height of near 16 km which caused them to overshoot the equilibrium level. Overshooting tops were also observed during the GATE experiment (Leary and Houze, 1979) and are common for mid-latitude squall-lines. The maximum radar reflectivity values for the overshooting cells of lines 1 and 2 were near 35 dBZ. This value is somewhat lower than typical values for GATE cells discussed by Leary and Houze (1979). They found maximum dBZ values from approximately 36 dBZ to 51 dBZ for the cells of 5 September 1974. The maximum reflectivity values for EMEX 2 were very comparable with the other EMEX days. For most of the convective lines examined during EMEX, the maximum reflectivity level was between 35 dBZ and 39 dBZ. During EMEX 3 and 6, there were higher reflectivity values. The maximum reflectivities for these flights were between 40 dBZ and 44 dBZ. The 35 dBZ maximum for the EMEX 2 convective line is significantly lower than the > 50 dBZ values of many mid-latitude squall-lines (Smull and Houze, 1987) which are likely due to hail.

Many of the cells comprising lines 1 and 2 were tilted parallel to the convective line as a result of the along line shear to be discussed in chapter 3. Figure 13 shows one of these sheared cells associated with line 1. In this case, the shearing was so extreme that the top of the sheared cell was advected above and precipitated into a forming cell possibly inhibiting the development of the
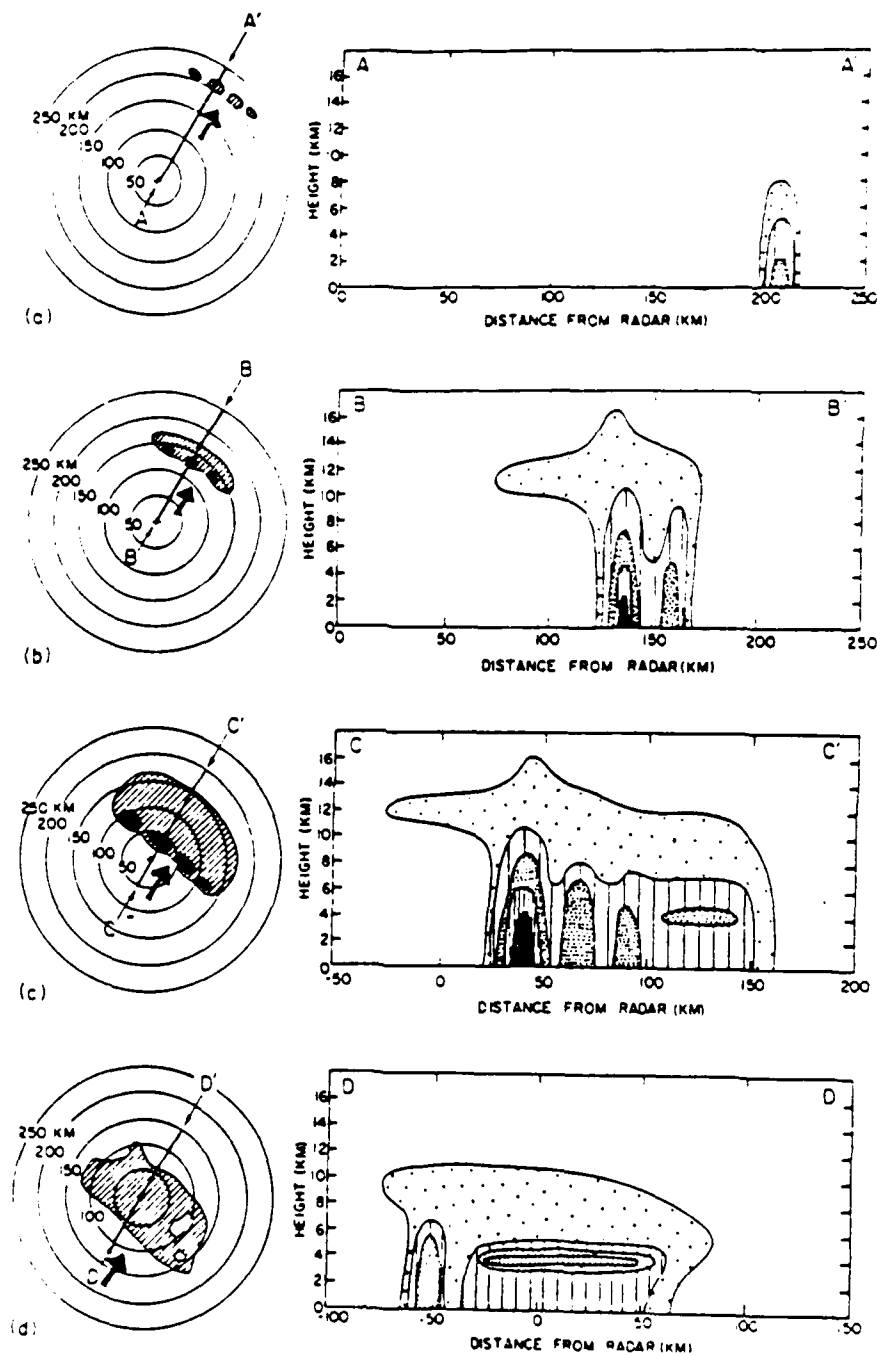
Figure 11: Schematic of a mesoscale precipitation feature during the (a) formative, (b) intensifying, (c) mature and (d) dissipating stages.. Heavy arrows on the horizontal cross section indicate direction of low-level flow, from Leary and Houze (1979).
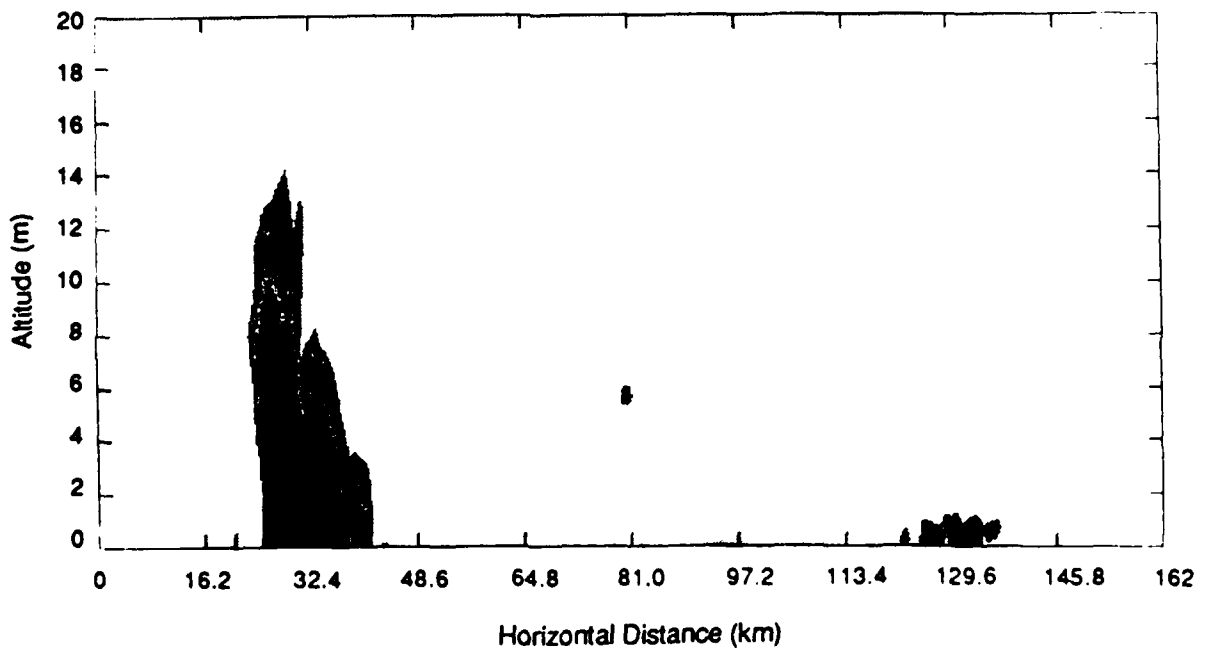
Figure 12:   Composited RHI scan of line 1 from 2025 GMT to 2040 GMT. Contours are for
              11, 17, 24, 33 dBZ.
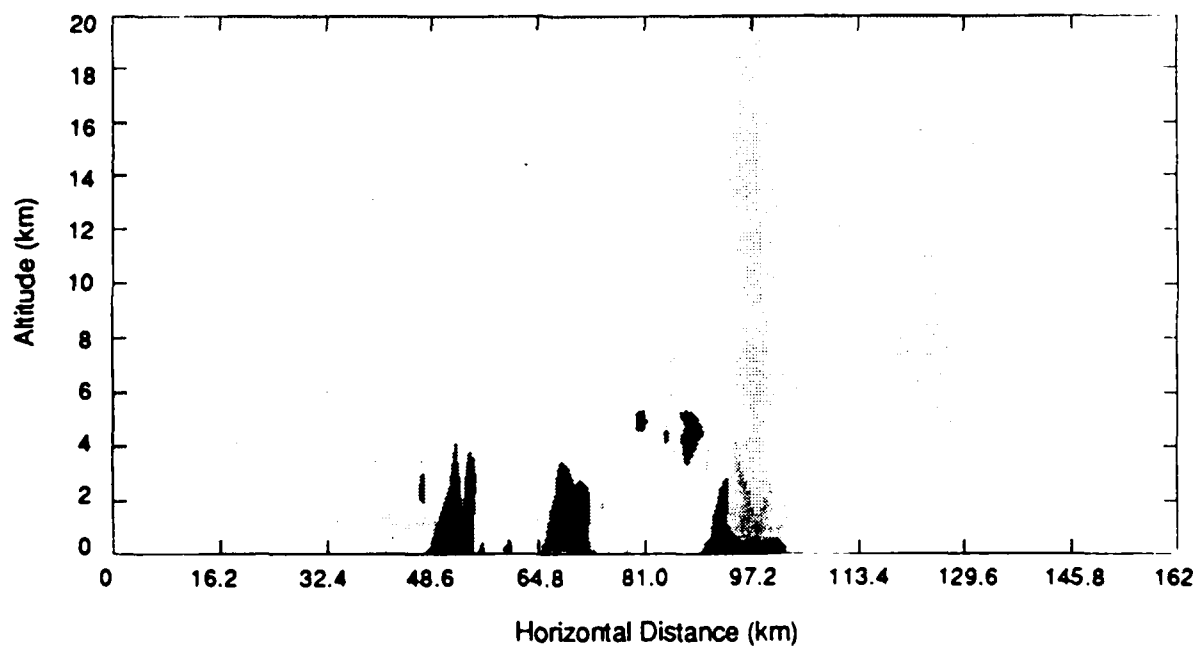
Figure 13:   RHI scan of a sheared cell along line 1 at 2255 GMT. Contours are for 11, 17, 24, 33 dBZ.

forming cell. From examing other RIII and PPI scans (not shown) in the vicinity of the sheared cell in figure 22, it appears that the portion of the cell which gave it a sheared appearance did not get advected into the region from flow in and out of the RIII scan.

As tropical convective lines enter the mature stage, they typically develop a nimbostratus anvil with a characteristic radar "bright band" as shown in figure 11. This nimbostratus anvil and bright band exists well after the convective portion of the line dissipates. Figures 14 and 15 depict a cross-sectional view of the mature stage of lines 1 and 2, respectively. Figure 14 shows no precipitation reaching the surface in the wake region and no well developed nimbostratus anvil. Figure 15 is much the same except a small amount of precipitation is reaching the surface in the wake region. However, a well developed nimbostratus anvil does not exist in line 2 either. The radar cross-sections presented in figures 14 and 15 are representative of lines 1 and 2 in the mature and dissipating stages. There was never any development of a well defined nimbostratus anvil or bright band associated with lines 1 and 2 of the EMEX 2 system. Thus, the EMEX 2 system does not fit into the life cycle categorization scheme of Leary and Houze (1979).

Because of the lack of nimbostratus anvil, the EMEX 2 convective line appears to warrant the addition of another class of convective lines to the Barnes and Sieckman (1984) scheme. This class would be for quasi-stationary, convectively dominated lines. Figure 16 is a graph of line speed vs. horizontal extent of nimbostratus anvil for tropical and mid-latitude convective lines reported in the literature. The data points where extracted from figures in articles by Chong (1987), Gamache and Houze (1982), Houze (1977), Houze and Rappaport (1984), Smull and Houze (1987), Zipser (1977), and Zipser et al. (1981). An F-test was conducted to see if there was any relationship between these two characteristics. A test of the null hypothesis of the slope being 0 was conducted, and the findings indicated there is a 96% confidence the slope is not 0. Thus, the data points in figure 16 have a significant relationship. With the slope that was calculated, the line through the data intercepted the y-axis at 2.09 ms^{-1}. It would be logical to define the quasi-
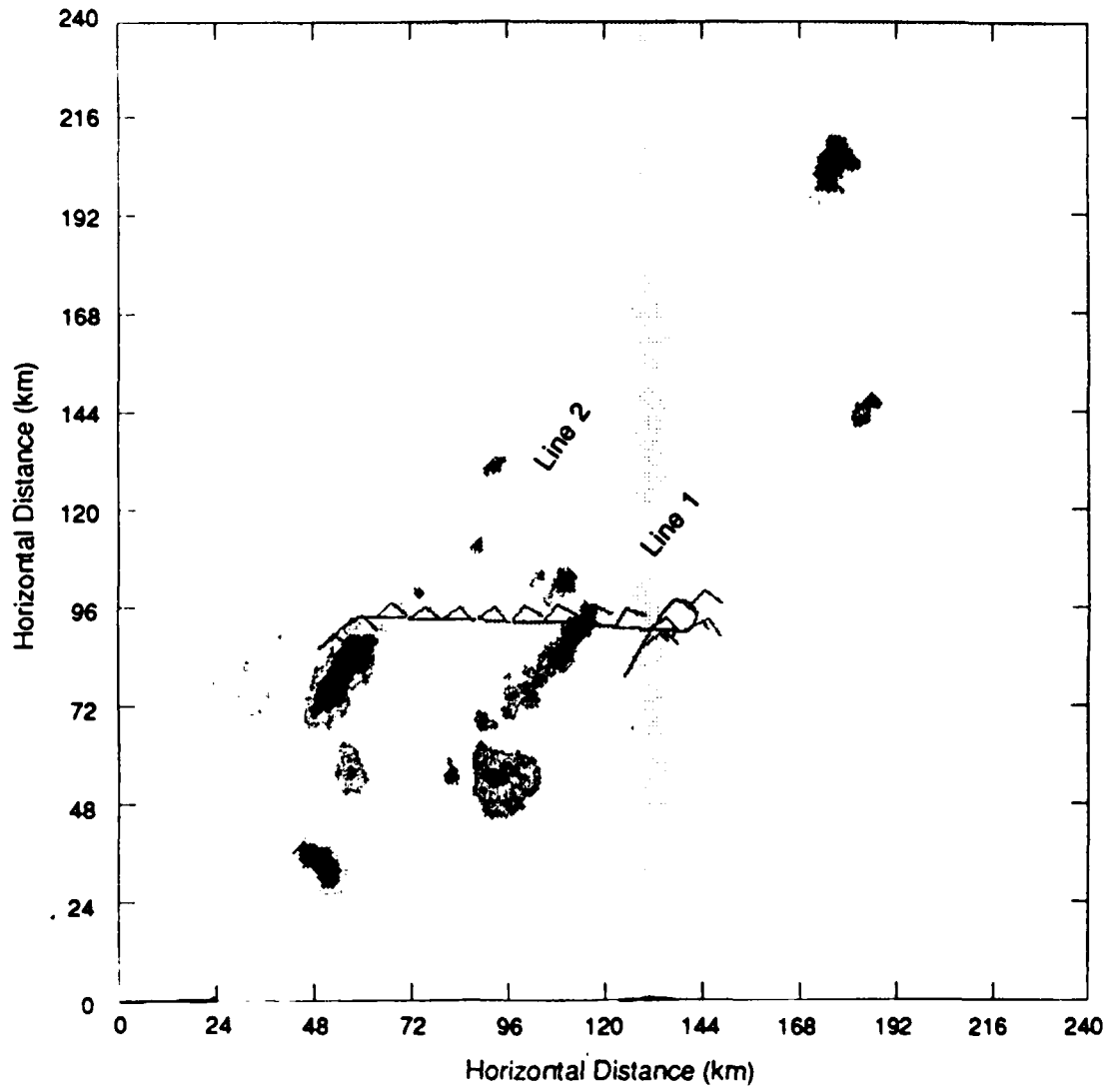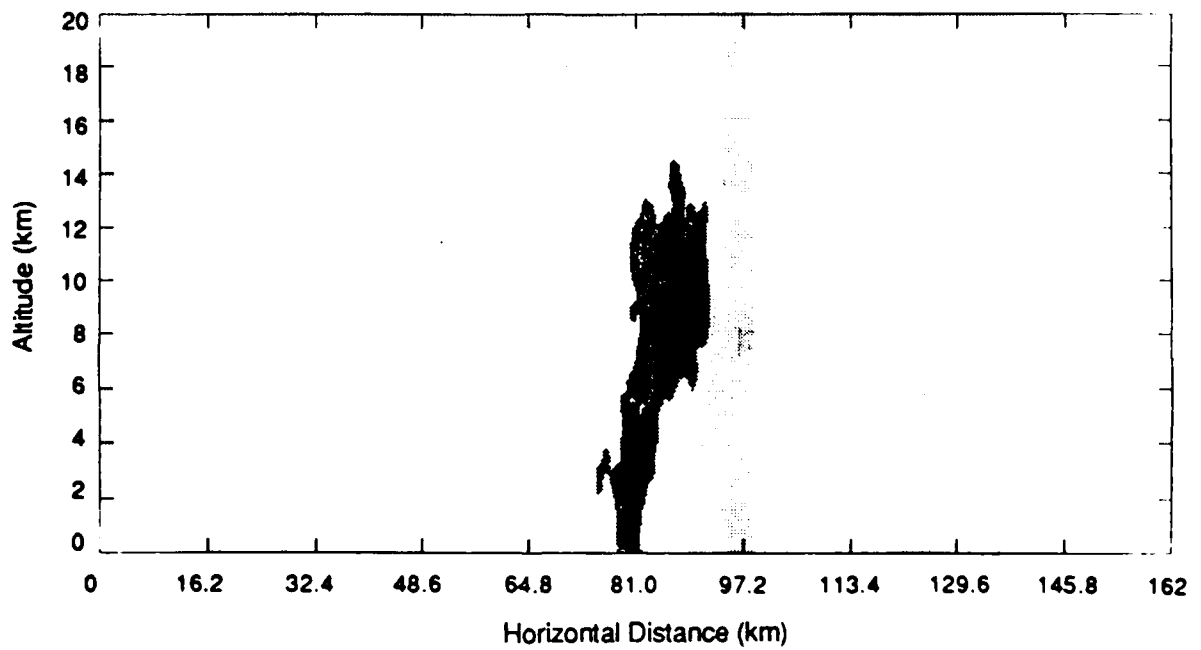
Figure 14:   PPI scan of line 1 at 2153 GMT. Contours are for 11, 17, 24, 33 dBZ.

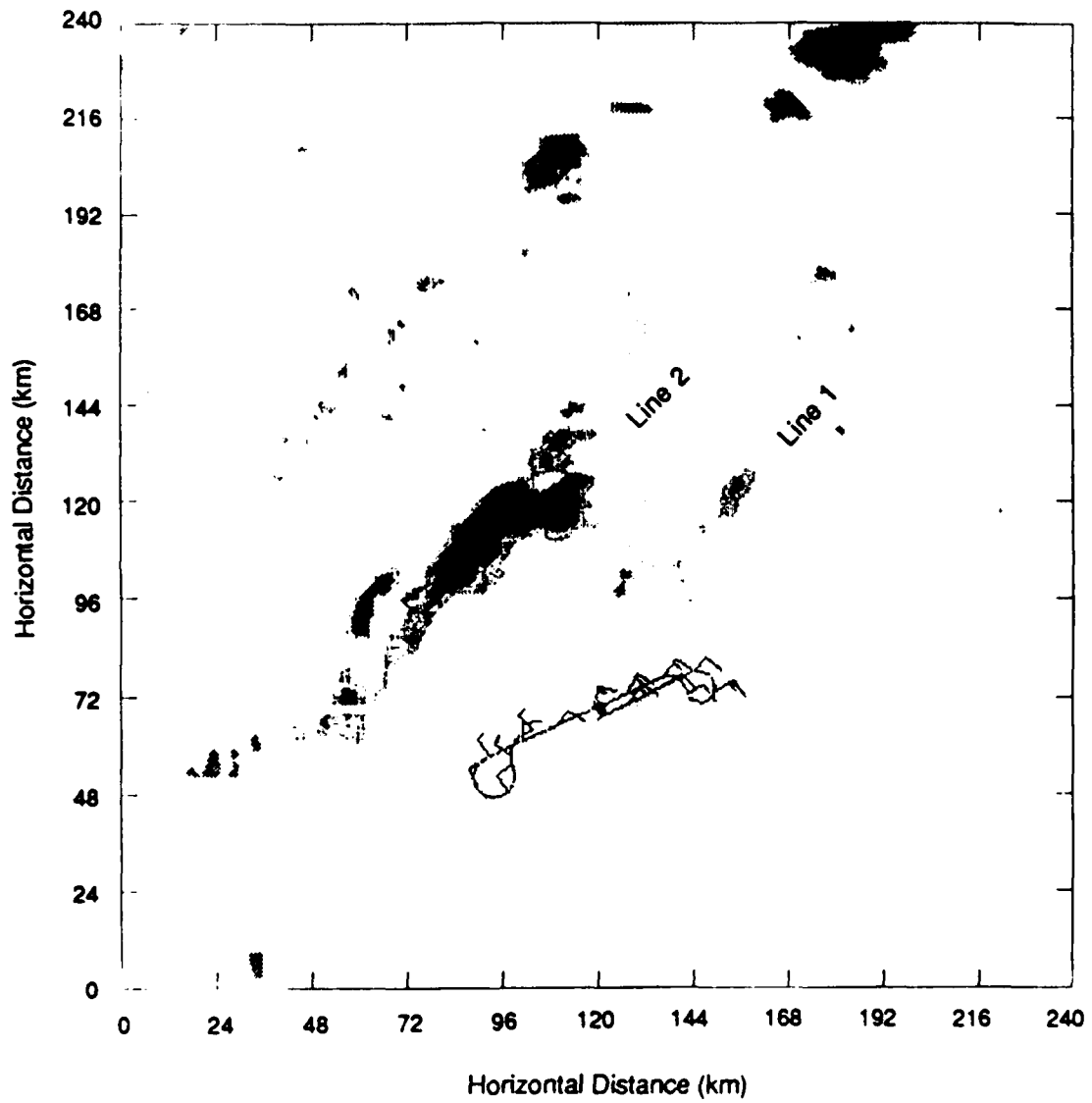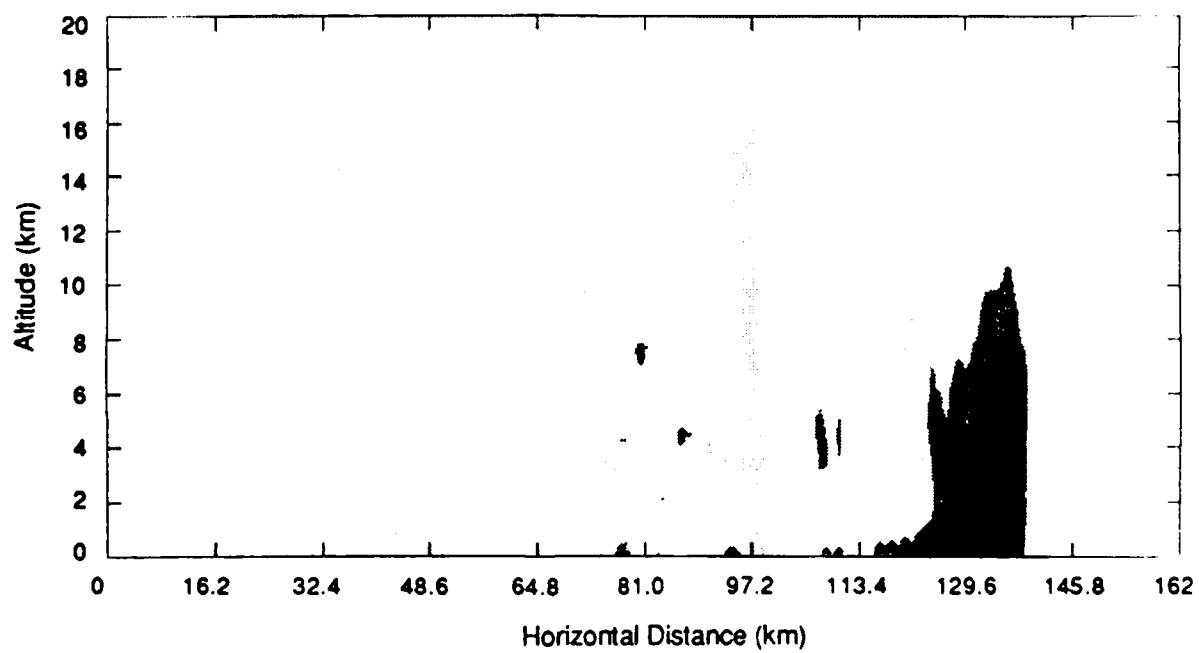Figure 15:   PPI scan of line 2 at 2321 GMT. Contours are for 11, 17, 24, 33 dBZ.
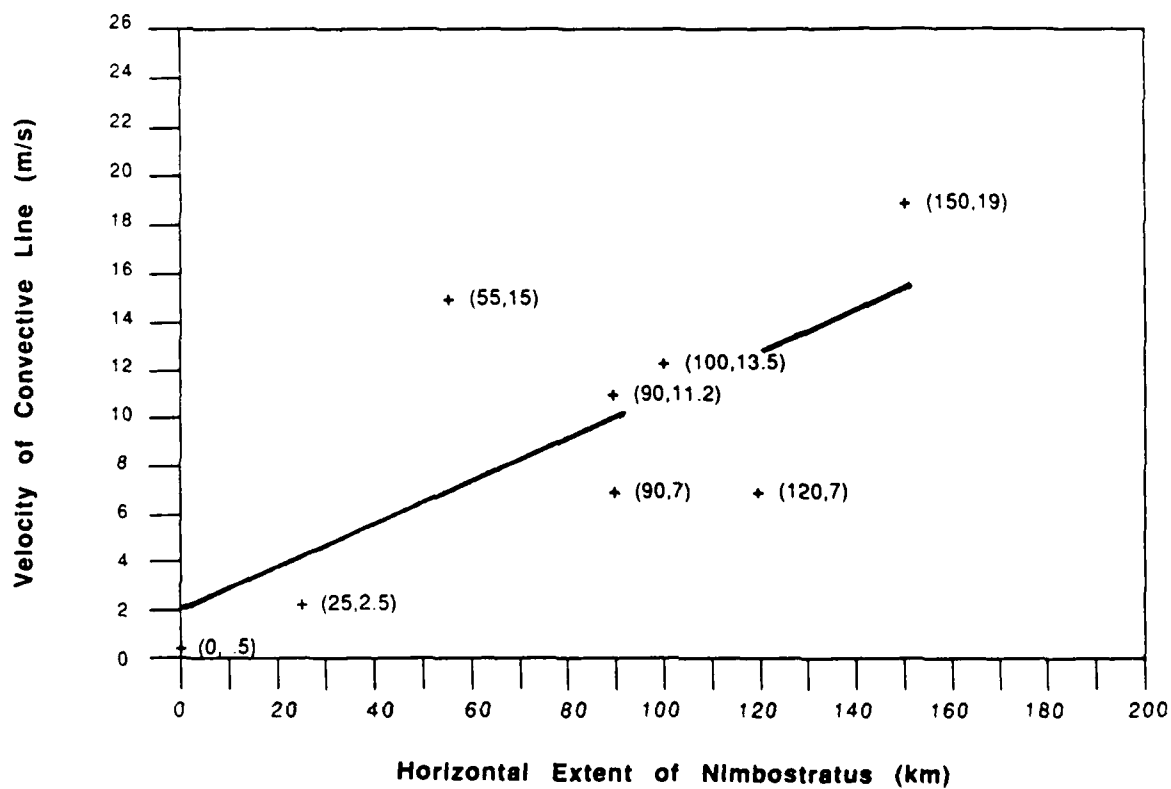
Figure 16:   Comparison of velocity of convective lines to nimbostratus anvil extent.

stationary category by the maximum speed associated with minimal nimbostratus production. This quantity, calculated from a least squares fit to the data in figure 16 is 2.09 ms^{-1}. However, there are not enough data points available from the literature to yield statistical confidence in this computed numerical value. Further studies of convective lines should increase the availability of the data needed for the definition of the quasi-stationary convective line category. Figure 16 shows a decrease in line speed is related to a corresponding decrease in the horizontal extent of nimbostratus anvil. The EMEX 2 convective line with little nimbostratus anvil and a line speed of 0.5 ms^{-1} is definitely in the quasi-stationary class suggested by the F-test results.

Parameterization of tropical convective lines in general circulation models could be improved by incorporating the observed relationships between environmental shear of v... line speed, and horizontal extent of nimbostratus anvil. The environmental shear of v_n controls the line speed, and the line speed and the environmental shear of v_n control the storm relative velocity profile which is the parameter of interest when considering moisture advection into the mesoscale stratiform region and, thus, the anvil extent. This addition to the parameterization algorithm would allow physically reasonable variation in the ratio of convection to stratiform precipitation, thus improving the parameterized latent and radiative heating profiles. Such improvements would contribute to a more realistic representation of the overall thermodynamics of the tropics. The results of Barnes and Sieckman (1984) suggest that a line speed parameterization could be based on the environmental wind profile, a quantity which is known in general circulation models.

Chapter 3

EMEX 2 ENVIRONMENTAL ANALYSIS

Barnes and Sieckman (1984) suggested that the type of convective line that forms on any particular day may be affected by the initial environmental conditions. With these results in mind it is the purpose of this chapter to examine the thermodynamic and kinematic structure of the mesoscale and synoptic scale environments associated with the EMEX 2 convective line.

3.1 Procedures for Sounding Compositing

Soundings for the environment and the wake regions were produced by combining all available proximity data. Data for the composite soundings came from flight level data from the NOAA P-3, the NCAR Electra, and the CSIRO Fokker along with data from the P-3's Omega dropwinsondes and rawinsondes from Gove and Thursday Island. The compositing of the wind direction and velocities was accomplished by vector averaging, whereas the thermodynamic variables were visually averaged using superimposed plots on a Skew-T, Log-P diagram.

For the composited environmental sounding below 500 mb the data from the Electra's descent and ascent near the line, the Omega dropwinsonde #4, and the Gove 1800 GMT and 0000 GMT soundings were used. Above 500 mb the 1800 GMT and 0000 GMT Gove soundings were used. At 500 mb all data sources matched the Gove soundings.

For the composited wake sounding below 950 mb, data from the Electra and the Fokker were used. From 950 mb to 400 mb, the data from the P-3 radiation sounding were used. Above 400 mb, the Thursday Island soundings from 1800 GMT/15 January and 0000 GMT/16 January were used for the composite. All the sources matched at the 400 mb level.

3.2 Environment vs. Wake Thermodynamic Profiles

Figure 17 is the composited thermodynamic and kinematic profile for the environment of the EMEX 2 convective line. It shows a deep layer of moist air from the surface to the upper troposphere. From composited thermodynamic data the environmental boundary layer depth was estimated to be 600m in depth.

The EMEX 2 thermodynamic profile is similar to those for fast-moving and slow-moving GATE convective lines composited by Barnes and Sieckman (1984). In each of the three cases a large amount of CAPE (1004 Jkg^{-1} to 1896 Jkg^{-1}) is present from approximately 900 mb to 200 mb, and a moist conditionally unstable boundary layer is present. The thermodynamic profiles from GATE and EMEX 2 are favorable for deep moist convection, even more so for the EMEX 2 case than for the GATE composites.

Figure 18 is the composited sounding for the wake region of the EMEX 2 convective line. The temperature and dewpoint profile for the EMEX 2 wake is noticeably different from the onion shape profile observed by Zipser (1977). GATE thermodynamic profiles from Zipser (1977) show a strong inversion from above the shallow cool boundary layer to approximately 900 mb with the dewpoint depression at that level being 15 °C. The EMEX 2 wake sounding below 900 mb shows no inversion, but it does have a stable layer between 955 mb and 910 mb with a maximum dewpoint depression of 4.2 K.

The most striking difference between the environmental thermodynamic profile and the wake thermodynamic profile is the potential buoyancy of a boundary layer parcel for each case. The level of free convection (LFC) for the EMEX 2 environment thermodynamic profile was 905.6 mb while the LFC for the wake region was 735.6 mb. The low altitude of the LFC for the environment leads to a low negative CAPE value of -12.3 Jkg^{-1}. The high altitude of the LFC in the EMEX 2 wake region leads to a deep layer of negative buoyancy below 735.6 mb. The CAPE
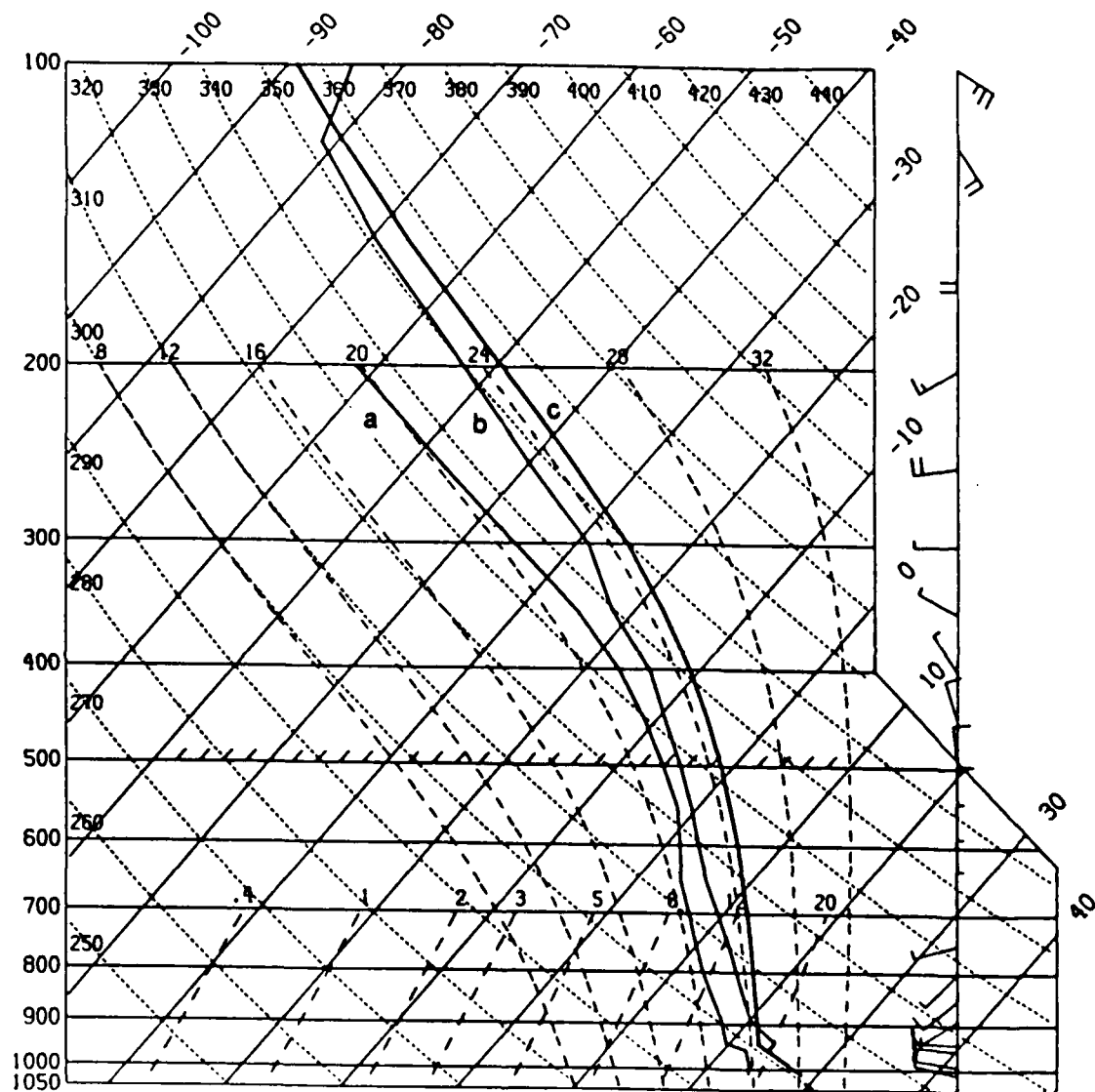
Figure 17:   EMEX 2 environmental sounding where lines a and b are the dewpoint and the temperature profiles respectively.. Line c represents the adiabatic ascent of a parcel. For the winds a full barb equals 10 ms⁻¹ and a half barb equals 5 ms⁻¹.
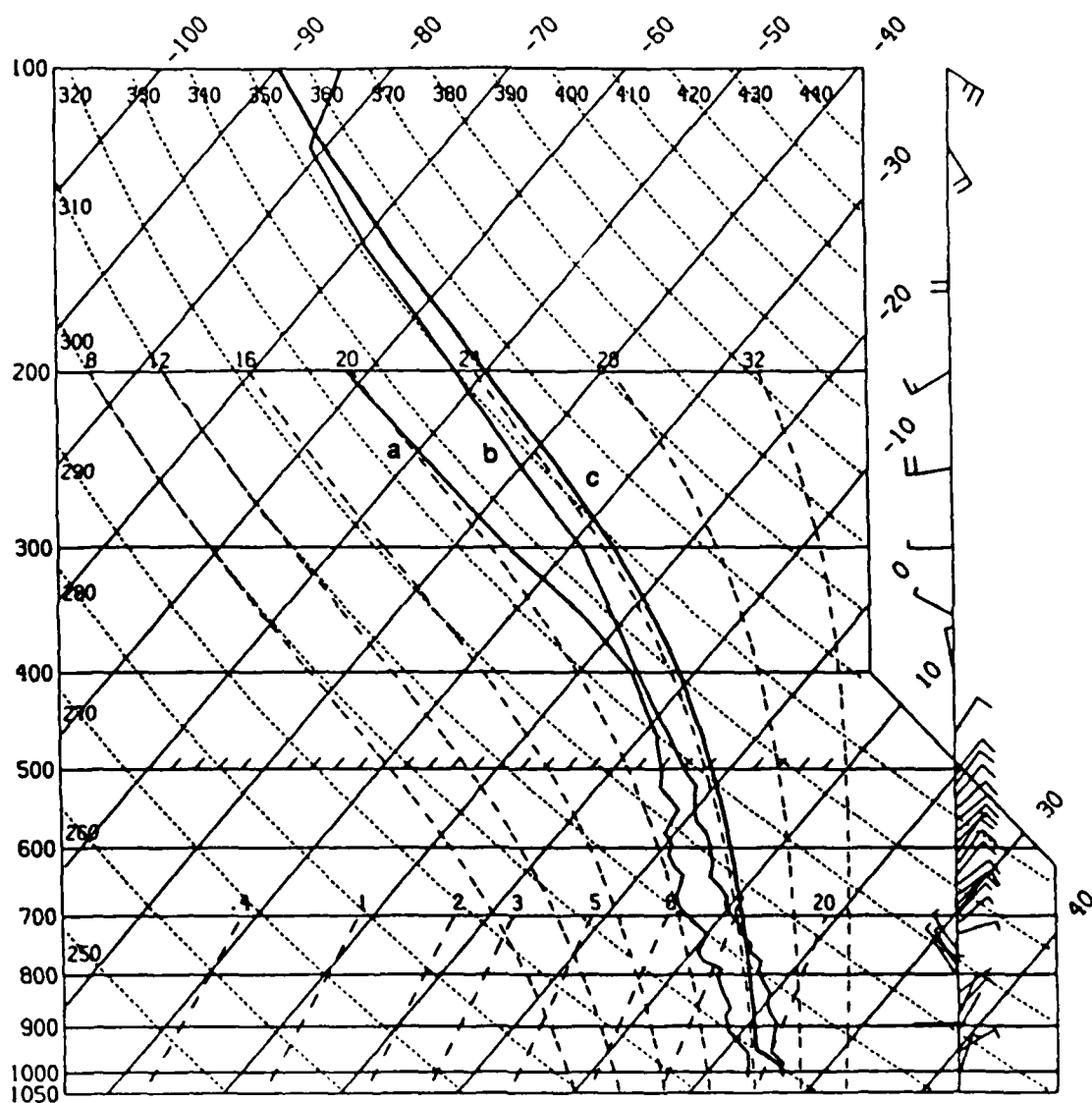
Figure 18: FMEX 2 wake sounding where lines a and b are the dewpoint and the temperature profiles respectively. Line c represents the adiabatic ascent of a parcel. For the winds a full barb equals 10 ms⁻¹ and a half barb equals 5 ms⁻¹.

of this layer was calculated to be -93.9 Jkg^{-1}. The greater lapse rate between 900 mb and 600 mb

for the environmental sounding resulted in a 26.8% difference in CAPE from the LFC to the EL

(Equilibrium Level) between the EMEX 2 environment and wake soundings with the

environment having the larger value of 1896.0 Jkg^{-1}. For the composited GATE slow-moving line

the difference in CAPE between the environment and the wake was 66.5% and for the

composited fast-moving line the difference was 93.2%. Thus, there appears to be a systematic

increase in the CAPE difference between the environment and the wake as the line speed

increases. For GATE, there may have been an under sampling of the wakes of slow-moving lines

via soundings which would cause the temperature and dewpoint readings to be too large thus

making the CAPE in the wake region too large (Barnes, personal communication, 1989).

3.3 Environment vs. Wake Wind Profiles

Figure 19 shows the wind component normal to the leading edge (v_n) of the EMEX 2

convective line. There is a strong negative wind shear of v_n from 960 mb to 850 mb. This is

significantly different from the positive wind shear of v_n for a GATE fast-moving line composite

(fig. 2) and the negligible shear case of the GATE slow-moving line composite (fig. 3) of Barnes

and Sieckman (1984). Above the freezing level, approximately 600 mb, the line normal wind shear

is very small for the EMEX 2 convective line up to 200 mb and is less than the line normal wind

shear for the GATE slow-moving line. The GATE fast-moving line had a negative line normal

wind shear from the freezing level to 5.8 km, and from 5.8 km to 9.6 km there was approximately

no line normal shear.

The important parameter for the advection of moisture from the convective region into the

mesoscale stratiform anvil region (to allow for the production of a nimbostratus anvil) is the

storm relative velocity (v_n-v). The crucial layer for this advection is from the freezing level to 10
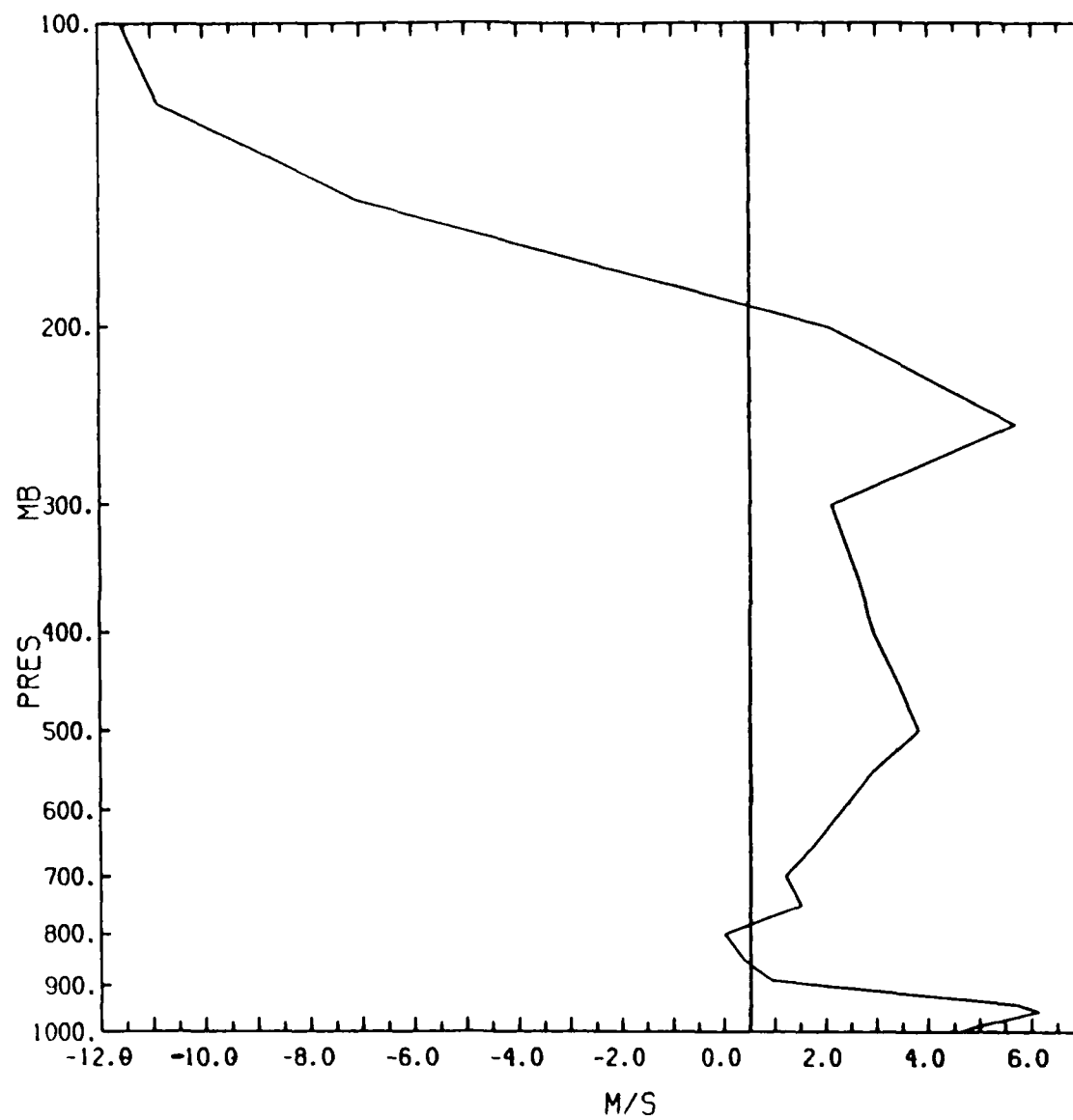
Figure 19:   EMEX 2 environmental v_n. The line speed of 0.5 ms^{-1} is indicated with a vertical line.

km ($\sim$ 290 mb). The freezing level bound is based on the crucial role of ice physics in the anvil thermodynamics. However, the 10 km level was chosen somewhat arbitrarily. Water content usually decreases with height, thus the 10 km level is a reasonable upper limit to a critical layer since moisture advection into the mesoscale stratiform anvil region above 10 km would be limited.

As stated in Section 1.2, v_n-v for the GATE fast-moving convective line became positive above 4.4 km allowing for moisture advection into the mesoscale stratiform anvil region. The storm relative velocity was 0.5 ms^{-1} at 4.4 km. At 5.4 km, v_{n-v} was 5.5 ms^{-1} and it reached a maximum of 7.5 ms^{-1} at 10 km. Figure 3 shows that v_n-v throughout the layer from the freezing level to 10 km was less for the slow-moving GATE composite than for the fast-moving composite. For the EMEX 2 convective line, v_n-v never is greater than 3.5 ms^{-1} from the freezing level to 10 km. The relative velocity for the entire layer between the freezing level and 10 km was less than the v_n-v for the GATE slow-moving convective line. The advection of moisture into the mesoscale stratiform anvil region is a function of line speed and of environmental shear of v_n which controls the storm relative velocity. The storm relative velocity controls the advection of moisture into the mesoscale stratiform anvil region.

The environmental profile of the velocity parallel (v_t) to the EMEX 2 convective line (fig. 20) indicates a low level maximum of v_t at 960 mb. From 975 mb to 500 mb the along line shear for the EMEX 2 case was 0.0015 s^{-1} compared to a 0.0013 s^{-1} for the GATE slow-moving composite and 0.0003 s^{-1} for the GATE fast-moving composite. These data suggest that the along line shear is inversely correlated with decrease in line speed.

3.4 Synoptic and Mesoscale Environment

At 0000 GMT on 15 January 1987 a surface cyclone was located southwest of Darwin (at the left edge of fig. 21). A monsoon trough extended northeast from this low into the Gulf of
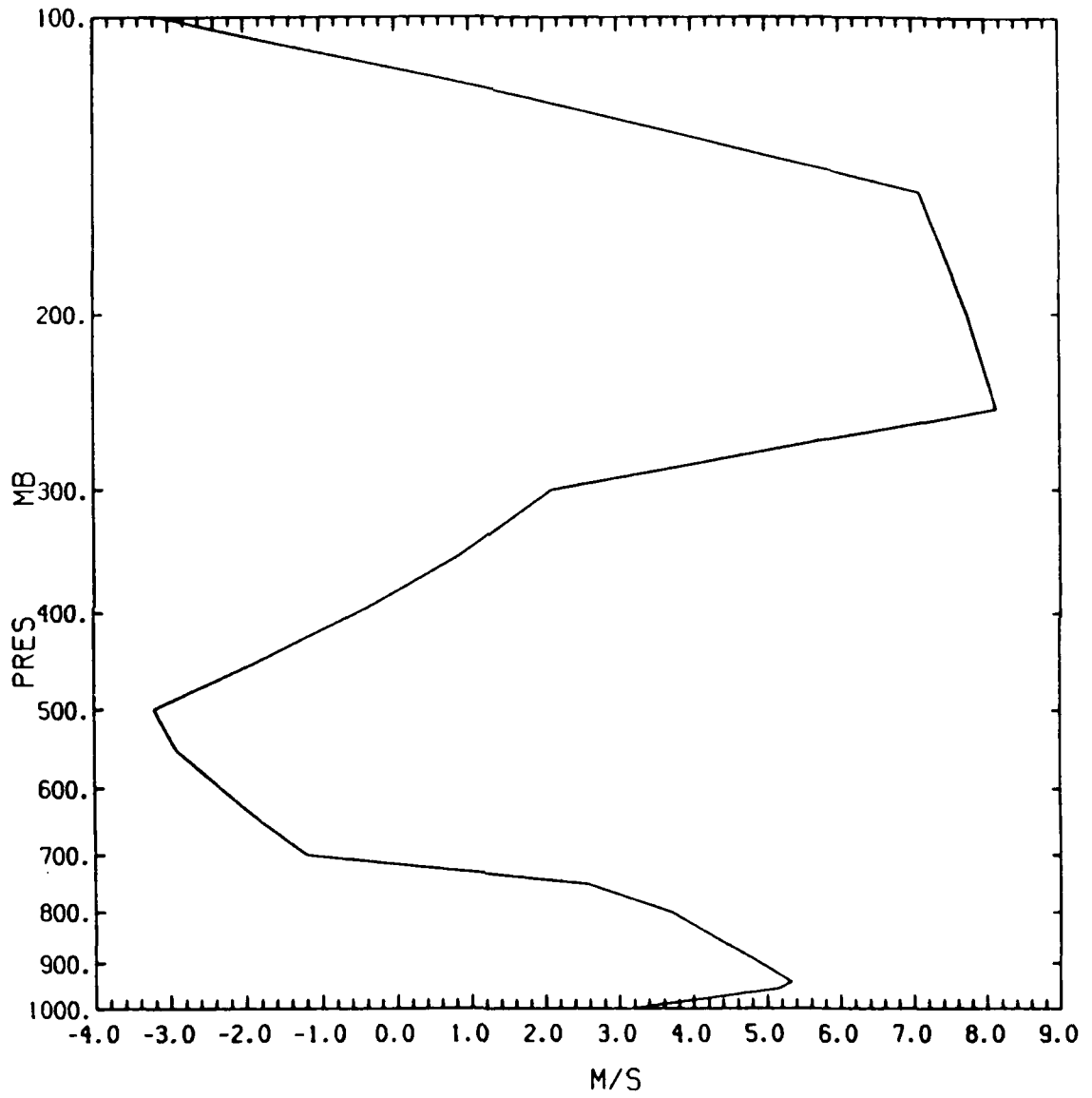
Figure 20: EMEX 2 environmental v_t profile.
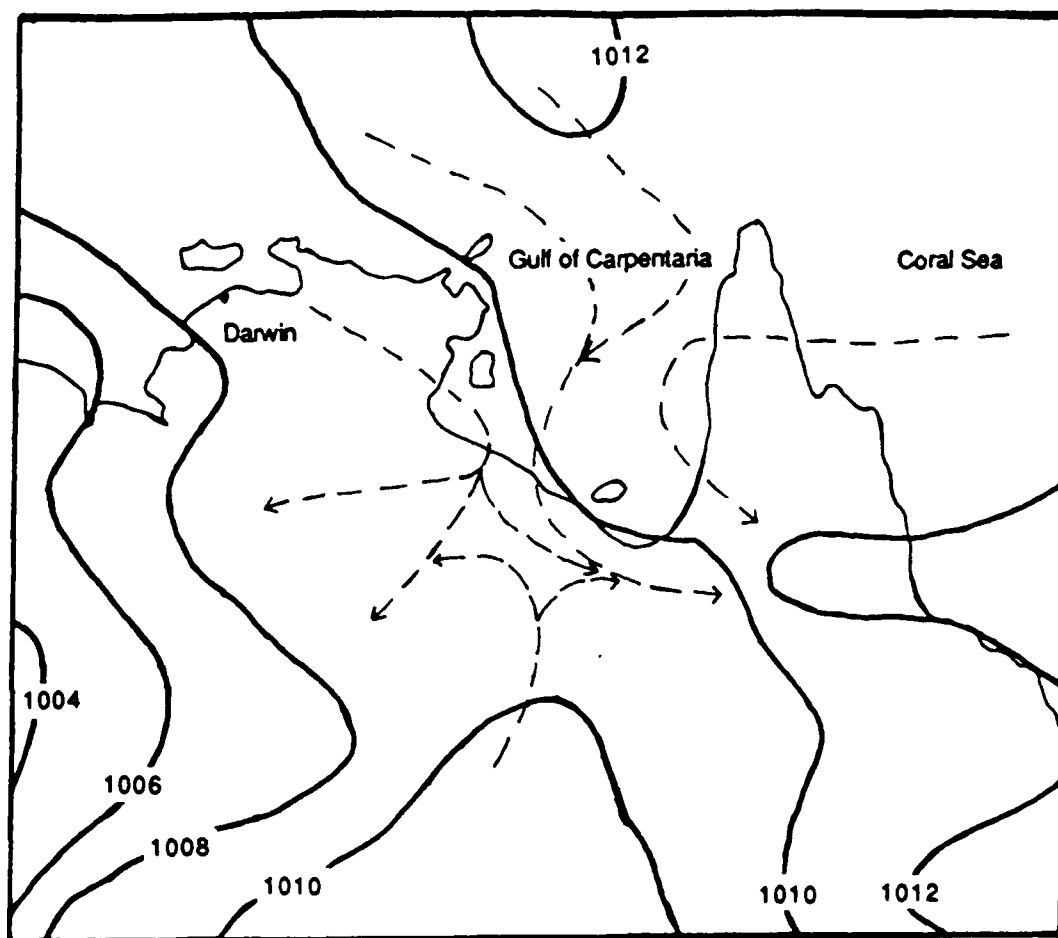
Figure 21: 0000 GMT/15 January 1987 surface chart with contours in millibars.. A cyclone was southwest of Darwin. Surface flow is represented by dashed lines.

Carpentaria. A northwesterly monsoon flow existed north of the trough. A northeast flow coming from the Coral Sea was entering the gulf southeast of the trough. The meeting of the two flow regimes along the trough axis provided an area of convergence in the middle of the gulf favorable for convective development. At the 200 mb level, an anticylone was centered over the mouth of the Gulf of Carpentaria suggesting ample divergence at this level (fig. 22).

At 0000 GMT on the 16th the surface cyclone was stationary and the northeastward extending monsoon trough still was present in the Gulf of Carpentaria (fig. 23). As a result, the strong convergence in the gulf from the northwest monsoon flow and the northeast flow from the Coral Sea still existed. At 200 mb the high pressure center had moved west of the Gulf of Carpentaria, suggesting decreased upper level divergence over the gulf area (fig. 24).

The low level mesoscale environment was examined using flight level data from the NCAR Electra. The data used were from a triangle pattern (fig. 25) flown around the central segment of the convective line just prior to the Electra's return to base. The convective line was located along the line of convergence shown in the 950 mb streamline analysis (fig. 26). The northwesterly monsoon flow is evident in the northern portion of the mesoscale area. The monsoon flow is advecting moist air into the mesoscale region with mixing ratios (W) ranging from 18.5 gkg^{-1} to 21.2 gkg^{-1}. The northeast flow from the Coral Sea also is important to the mesoscale area with W of 18.0 gkg^{-1} to 20.5 gkg^{-1} being advected into the mesoscale region by this flow.

The convective line developed along the monsoon trough which separated the monsoon flow from the northeast flow off the Coral Sea. The 950 mb streamline analysis shows inflow on both sides of the convective line with inflow velocities of 4.2 ms^{-1} to 7.6 ms^{-1} to the northwest of the line and of 0 ms^{-1} to 3 ms^{-1} to the southeast of the line. Also analyzed in the 950 mb streamline field is a mesoscale cyclone which will be discussed in chapter 4. The moist inflow on both sides of the monsoon trough is ideal for the enhancement of convection along the trough.
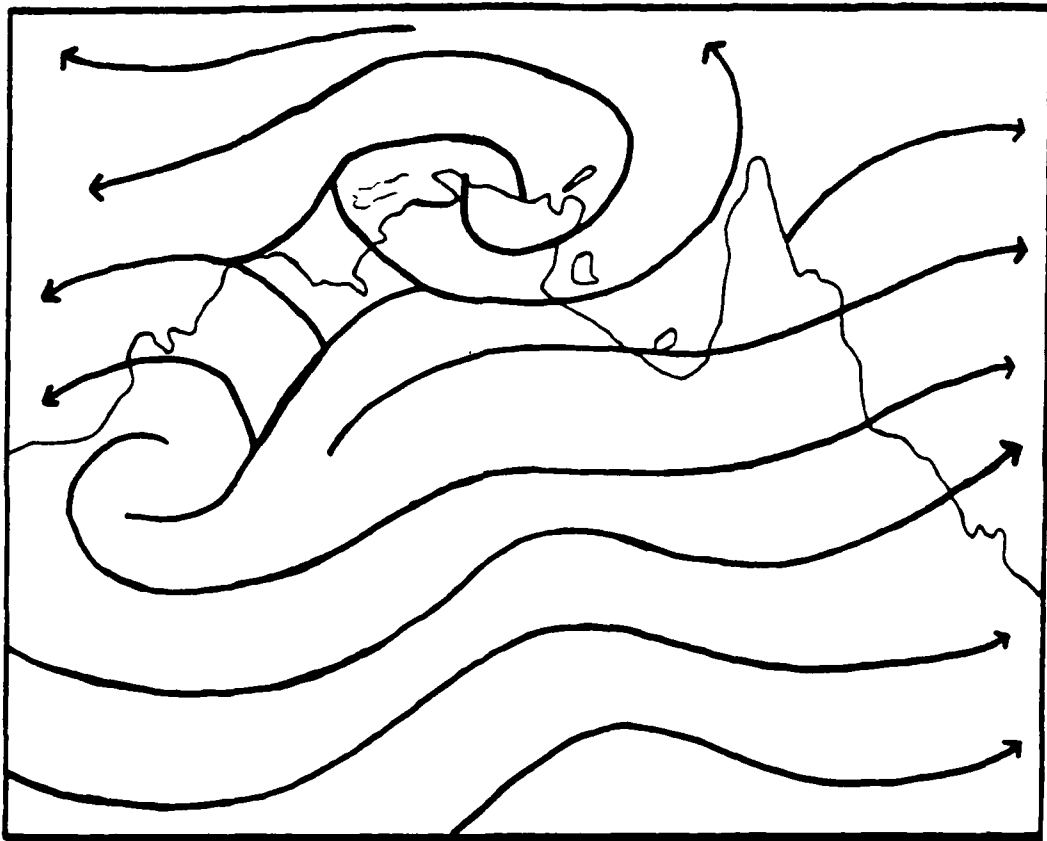
Figure 22:   0000 GMT 15 January 1987 200 mb streamline analysis.
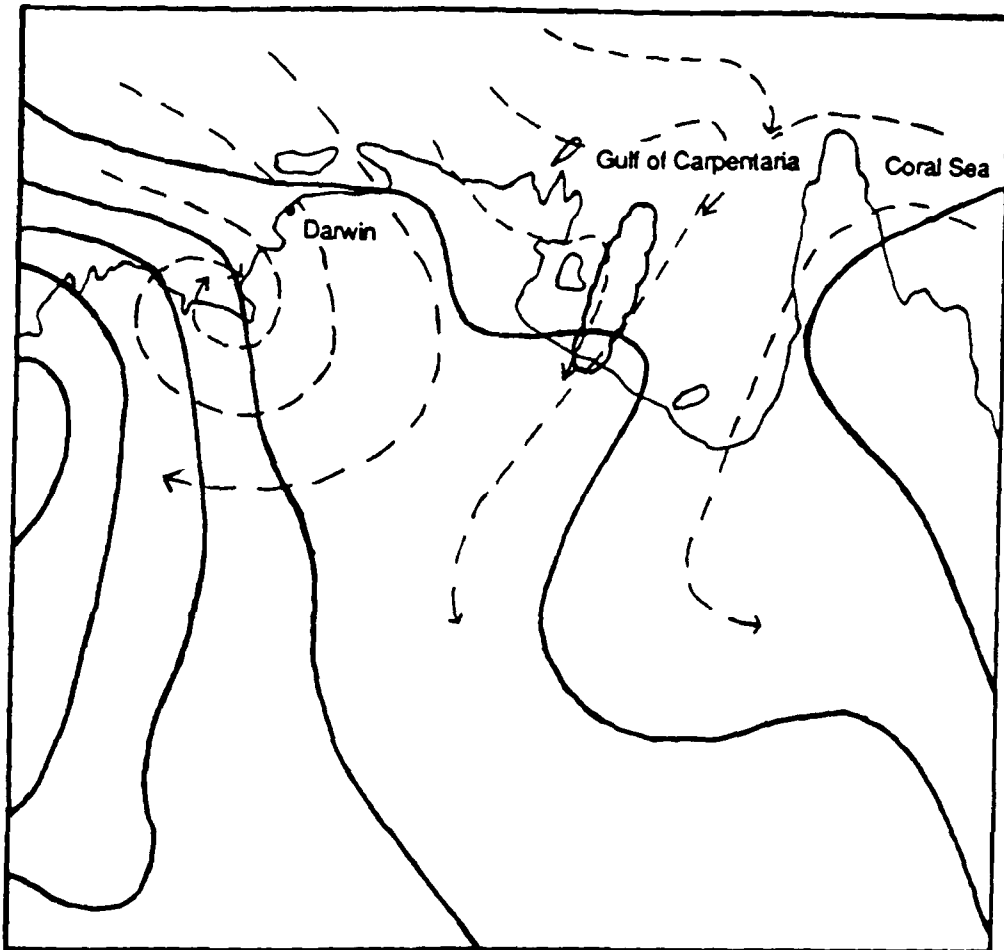
Figure 23:   0000 GMT/16 January 1987 surface chart with contours in millibars.. A cyclone was southwest of Darwin. Lines 1 and 2 are shown combined as scallops. Surface flow is represented by dashed lines.
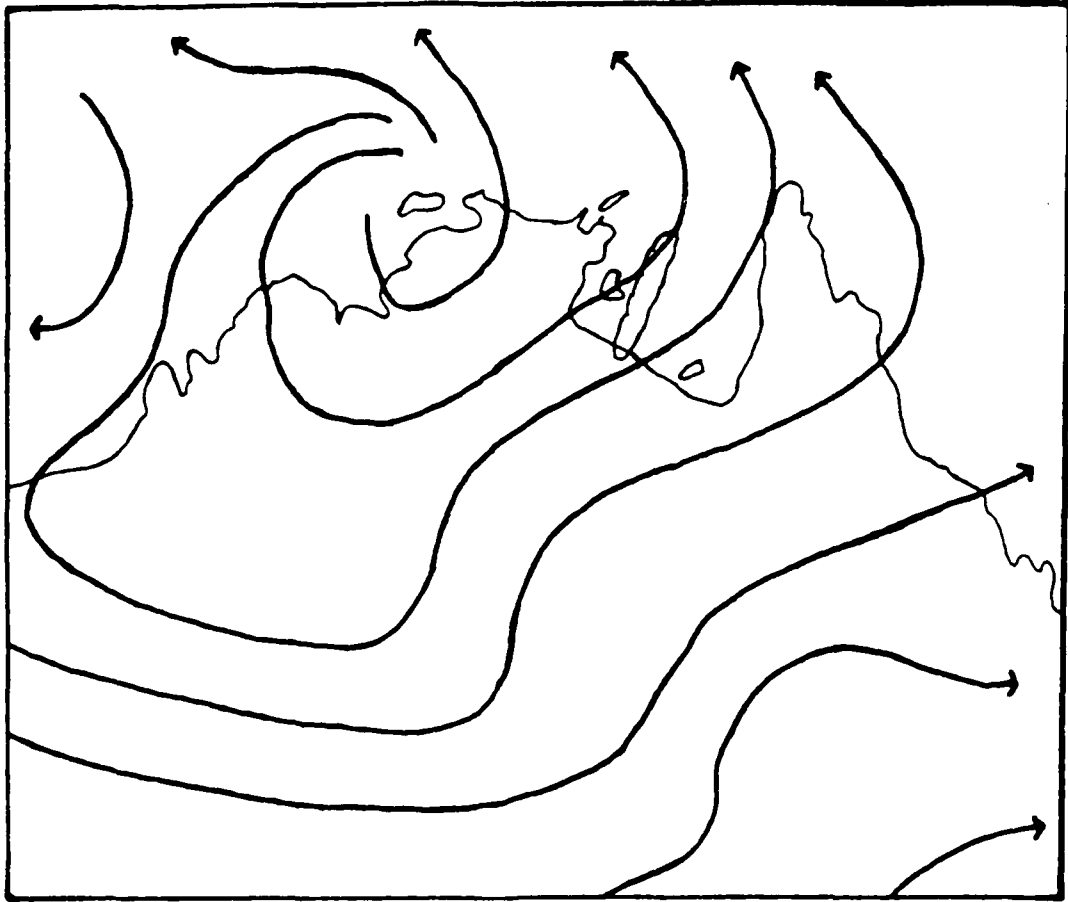
Figure 24:   0000 GMT 16 January 1987 200 mb streamline analysis. Lines 1 and 2 are shown combined as scallops.
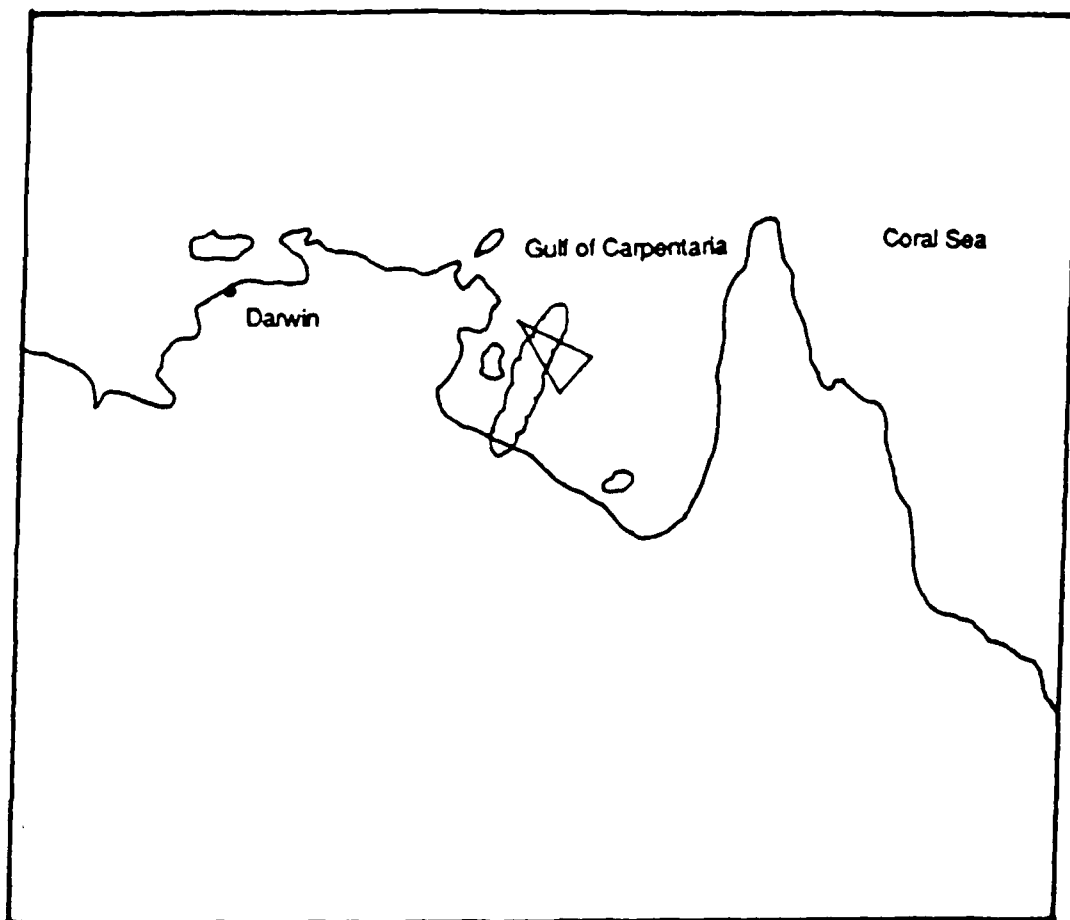
Figure 25: Shown is the triangle flight path of the NCAR Electra. Lines 1 and 2 are shown combined as scallops.
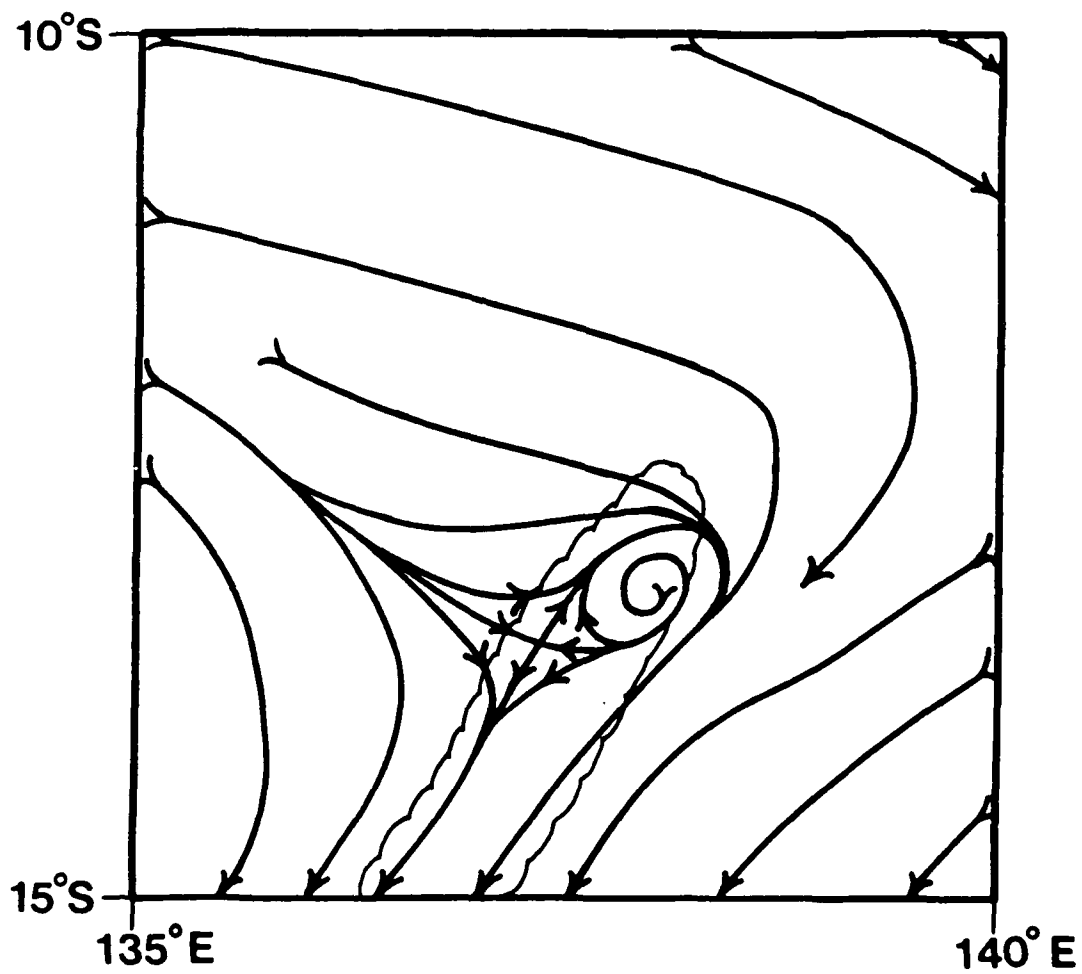
Figure 26:   950 mb streamlines from aircraft and rawinsonde data. Lines 1 and 2 are shown combined as scallops.

Chapter 4

COMPOSITED STORM STRUCTURE

A review of composited aircraft data for the EMEX 2 convective system will be accomplished in this chapter. The goal is to develop a conceptual model of a quasi-stationary convective line. Data from lines 1 and 2 were composited together because of the similarities of the two convective lines.

4.1   Procedures for Compositing Aircraft Data

Composited cross sections were prepared for vertical velocity (w), horizontal velocity normal (v_n) and tangential (v_t) to the convective line, mixing ratio (W), equivalent potential temperature, and virtual temperature (T_v) (fig. 27). The data used were flight level data from the NCAR Electra collected at 1 Hz and 20 Hz depending on the sensor. The final processed data for each composite were in the form of 5 second averages of these high rate data. The normal and tangential velocities were determined geometrically by using 5 second averages of 20 Hz wind speed and direction data. The mixing ratio is in terms of grams of water vapor per kilogram of dry air. The equivalent potential temperature was obtained using the method presented by Bolton (1980). T_v was calculated using the method discribed in the Smithsonian Meteorological Tables (1966). In situ sensors provided the kinematic (gust probe/inertial navigation system combination) and thermodynamic (Rosemont type 102 thermometer, thermoelectric dewpoint hygrometer) values at flight level.

During EMEX 2, the NCAR Electra flew flight legs that concentrated on the environment, the convective region, and the wake region of convective lines 1 and 2. These legs were oriented perpendicular to the lines. Legs were flown at elevations of approximately 200 m and 520 m for

Figure 27: Composite of T_v (°C) for the FMEX 2 convective line from 200 m to 3200 m. The leading edge of the convective line is at 20.3 km.

line 2, and 1200 m, 2000 m, and 3200 m for line 1. The flight level data were processed to produce constant height composites for each of these levels. These constant height composites were then used to produce a composited cross section of the EMEX 2 convective lines.

The data from each flight leg were projected onto a straight line extending from a predetermined reference point at a specific latitude and longitude perpendicular through the convective line. Data from the individual flight legs were synchronized with data from the other flight legs at the same altitude by aligning the projected location of the leading edges of the convective lines. Based on information from the video recording taken from the NCAR Electra and position data from the inertial navigation system, the gust front was found to be within 0 km to 2 km ahead of the main convective updrafts associated with lines 1 and 2. Thus, the gust front and the leading edge of the deep convection were virtually co-located for the EMEX 2 system. The system's leading edge was located by examining the video recording for arcus and looking at the kinematic and thermodynamic data for gust front and cumulonimbus leading edge type signatures. A bin average was performed to obtain the final constant height composite. The bin average was performed by using a bin width of 0.55 km corresponding to approximately 5 seconds of aircraft data. After all the constant height composites were completed, they were aligned vertically with respect to the leading edge at each level, and the composite cross section was produced. At low levels, the storm was observed to tilt somewhat with height. Thus, the leading edges for each level were not vertically stacked in reality. However, aligning the leading edges vertically was felt to be the best method because the exact tilt of the leading edge can not be determined for broken lines such as those observed during EMEX 2.

4.2 Composite of Vertical Velocity (w)

The vertical velocity for 5 levels from 200 m to 3200 m (fig. 28) for the environment, and the convective region will be reviewed. Origins of updraft and downdraft air will be determined using the equivalent potential temperature composite (fig. 29). Sensor wetting of the temperature and dewpoint instruments was not corrected for. Therefore, the equivalent potential temperature values in the convective region are anomalously high. Comparison between the EMEX 2 system and GATE and mid-latitude convective lines will be made where appropriate.

4.2.1 Updrafts in the Environment and in the Main Convection

Measurements indicate the composited vertical velocities in the environment were from -0.54 ms^{-1} to +0.70 ms^{-1}. Above the boundary layer, there was gentle subsidence with composited vertical velocities from 0.0 ms^{-1} to -0.6 ms^{-1}. Within the boundary layer, the structure of w was more complex. A positive surface flux of T_v, and thus buoyancy, was measured in the environmental boundary layer (discussed in more depth in chapter 5). This buoyancy flux supported the formation of thermals in the boundary layer. It is the motions of these boundary layer convective circulations which are contributing to variations in the composite at the 200 m and 520 m levels. The thermals in the environment were not strong enough by themselves to penetrate the inversion and produce vigorous moist convection. The mesoscale convergence zone discussed in chapter 2 and the gust front from previous convective cells were required to lift environmental boundary layer air to its LFC.

The convective region (from the leading edge to the back of the third secondary updraft) of the EMEX 2 case was approximately 20 km wide. Directly behind the leading edge of the composited convective line there was an updraft core, w > 1.0 ms^{-1}, (as defined by LeMone and Zipser, 1980) throughout the lower 520 meters of the atmosphere. However, at 1200 m and 2200
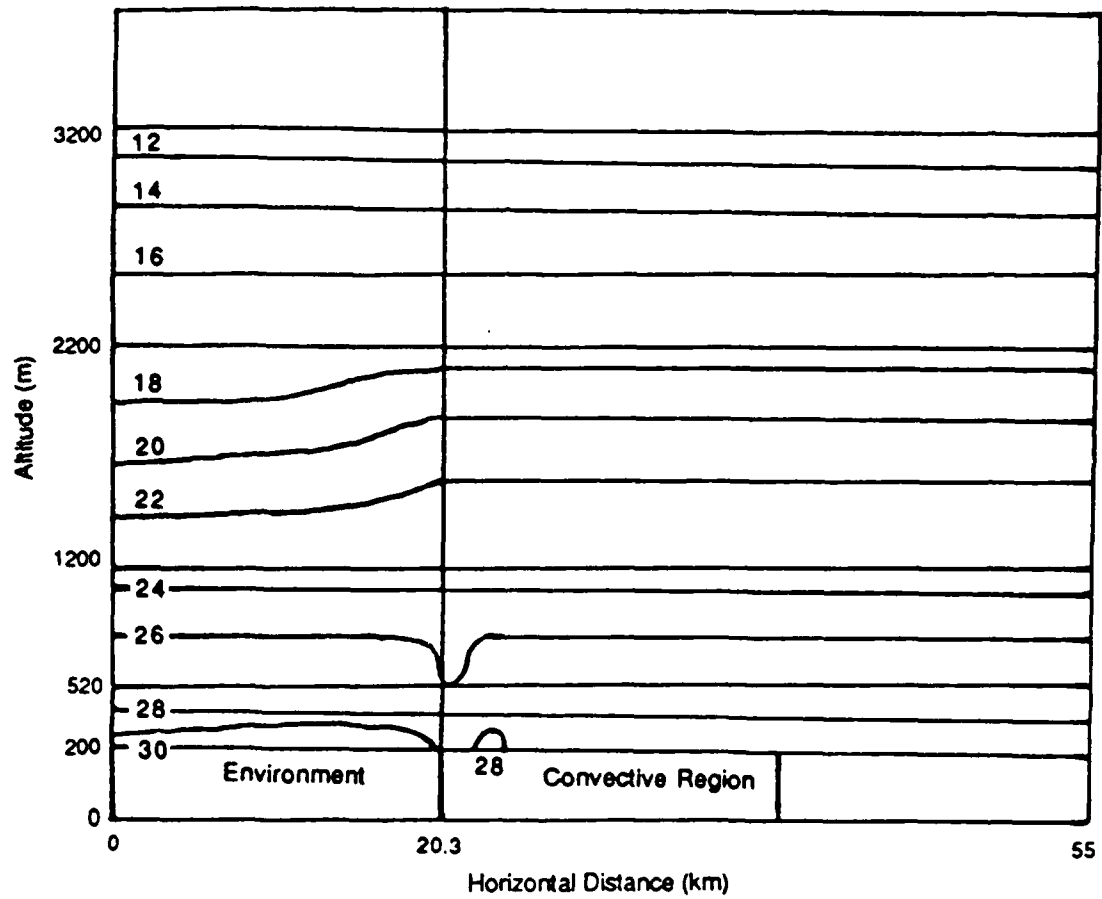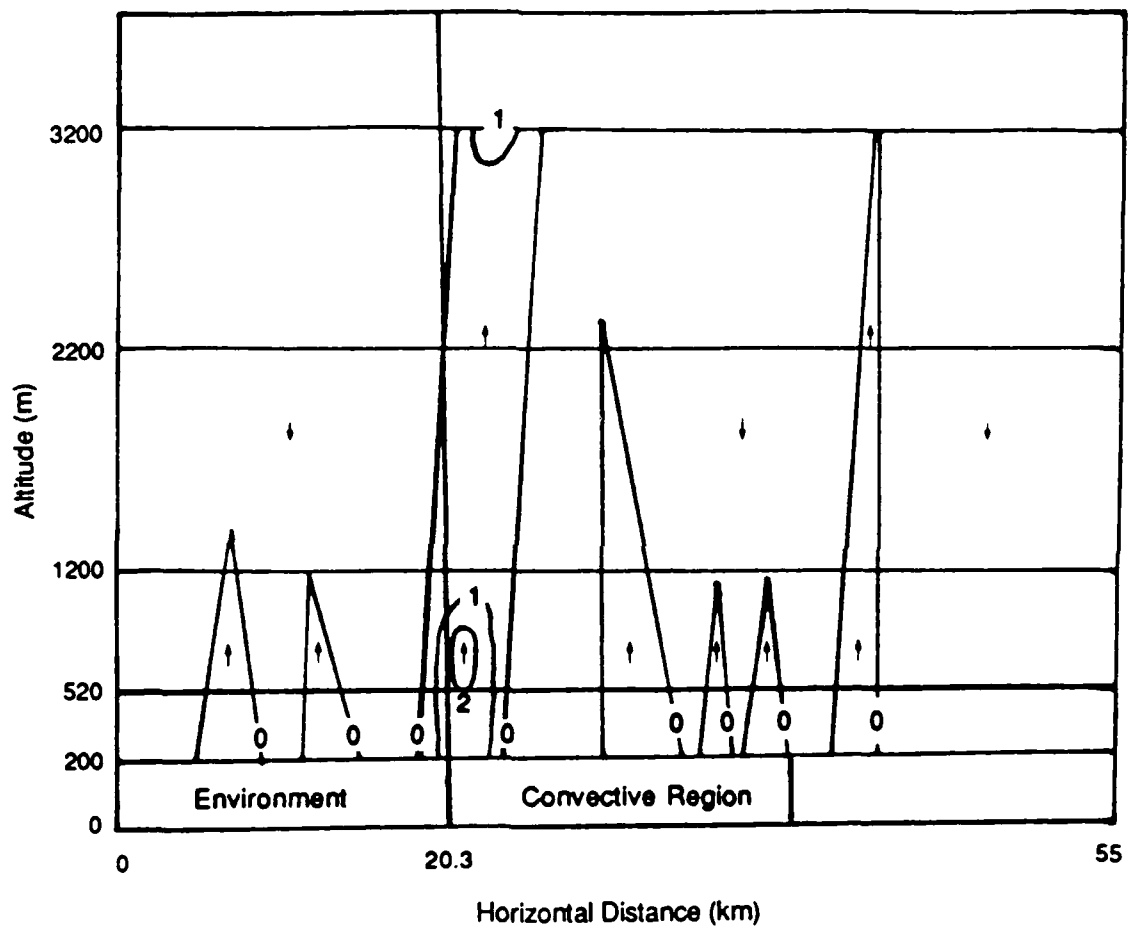
Figure 28: Composite of w (ms⁻¹) for the EMEX 2 convective line from 200 m to 3200m. The leading edge of the convective line is at 20.3km.

Figure 29: Composite of equivalent potential temperature (K) for the EMEX 2 convective line from 200 m to 3200 m. The leading of the convective line is at 20.3 km.

m, there were no composited updraft cores as w was $<$ 1.0 ms⁻¹ throughout the area. An updraft core directly behind the leading edge was reestablished at 3200 m with w > 1.0 ms⁻¹. The maximum composited w for the updraft was 2.75 ms⁻¹ at 520 m; however, the strongest 5 second average w in a convective region on 15 January 1987 was 4.8 ms⁻¹ at 3200 m. The variance of w was significant in the primary updraft region from the leading edge to 3.33 km behind the leading edge. At 3200 m, the maximum variance was 18.47 m²s⁻² located 1.5 km behind the leading edge. The variance for the 2200 m level was less with a maximum of 4.15 m²s⁻² located 2.22 km from the leading edge. The variance shows that there were variable updraft positions associated with different penetrations of lines 1 and 2. Thus, there is an underestimate of the updraft core strength by the composite. The variance is defined to be the sum of the squared deviations of the measurements about their mean divided by one less than the number of measurements.

4.2.2 Downdrafts in the Environment and in the Main Convection

The primary downdraft was weaker in intensity and covered a wider area than the primary updraft. The downdraft region in the lower 520 m was approximately 7 km wide. Although throughout the downdraft w was fairly uniform from 200 m to 3200 m, the most intense negative composited vertical velocity observed was -3.02 ms⁻¹ at the 200 m level. The variance of w in the downdraft region at the 2200 m and 3200 m levels was less than 1 m²s⁻² except for one 5 second average where it was 4.1 m²s⁻² at 2200 m near the boundary of the composited updraft and downdraft. The small amount of variance of w in the downdraft region is reasonable since there was only a small amount of negative buoyancy of the parcels in the downdrafts, and the downdraft cores needed to produce larger variance require more negative buoyancy.

The vertical velocities for the EMEX 2 system were comparable to those measured during GATE. LeMone and Zipser (1980) reviewed the intensity of the updrafts and downdrafts for 6 days of the GATE experiment and found that approximately 98.5% of the vertical velocities at

levels below 4300 m in the convective region were less than 4 ms⁻¹ with a maximum of near 6.5ms⁻¹. Thus, the EMEX 2 and GATE storms differ significantly from mid-latitude continental convective lines whose updrafts and downdrafts often have embedded cores with w > > 4 ms⁻¹ (Smull and Houze, 1987).

4.2.3 Origins of Convective Updraft and Downdraft Air

In the environment, there was no well defined vertical motion except in the boundary layer a few kilometers ahead of the leading edge. Updrafts in the environment associated with this low level convergence in the boundary layer resulted in a small region of cumulus extending ahead of the convective line.

The convective region displays a mixing of air with origins at a number of different levels and locations. The convective downdraft air at the 200 m level appears to have originated at many different levels in the environment. The equivalent potential temperature at this level would suggest that some of the convective downdraft air originated in the lower environmental boundary layer. This air would have been ingested into the updraft at 600 m or below and transferred to the downdraft as a result of the water loading contribution to net buoyancy. In the downdraft, some of this air did not mix with its surroundings and thus maintained its high equivalent potential temperature. Lower equivalent potential temperature values were also present in the downdraft at 200 m. With equivalent potential temperature values of near 345 K, this air would appear to have two possible origins. First it could be environmental air from near 2000 m which was ingested into the updraft then moved into the downdraft and finally descended to 200 m without mixing with the surrounding air. Another possible origin for this air would be the mixing of environmental boundary layer air from the updrafts with air from various levels of the environment at or above 2200 meters.

The downdraft air spread out near the surface towards the leading edge and the back of the convective region. Therefore, low equivalent potential temperature air was available to be lifted into the base of the main updraft. This downdraft air being mixed with high equivalent potential temperature environmental boundary layer air resulted in composited equivalent potential temperatures in the updraft core as low as 347.9 K. Examination of individual flight legs verified that low equivalent potential temperature air was rising in the convective updrafts, thus this result was not an artifact of the composite. Since the low equivalent potential temperature air in the main updraft did not reach the 1200 m level, it was probably confined to the gust front circulation.

4.3   Environmental Inflow

Environmental inflow will be examined in this section using the normal velocity (v_n) composite (fig. 30). The normal velocity is perpendicular to the convective line but is not storm relative.

Environmental inflow is important to the existence of a convective line because it advects moisture into the line at low levels permitting maintenance of the convective line through the release of latent heat. The EMEX 2 convective line was propagating to the northwest at $v = 0.5$ ms^{-1} which is defined to be in the negative x-direction in figure 30. Thus, inflow near the leading edge of the convection can be measured by v_n-$v > 0$. From approximately 200 m to 3200 m, the inflow within 7 km of the leading edge never exceeded $+6.1$ ms^{-1}. The greatest inflow occurred in the boundary layer with the maximum value near the top of the boundary layer. The inflow in the boundary layer advected air with W from 18.1 gkg^{-1} to 19.1 gkg^{-1} (fig. 31) into the convective line. This sustained inflow of moisture was a major reason why the convection was vigorous and long lasting on 15 January 1987.

Figure 30: Composite of v_n (ms^{-1}) for the EMEX 2 convective line from 200 m to 3200m. The leading edge of the convective line is at 20.3 km.
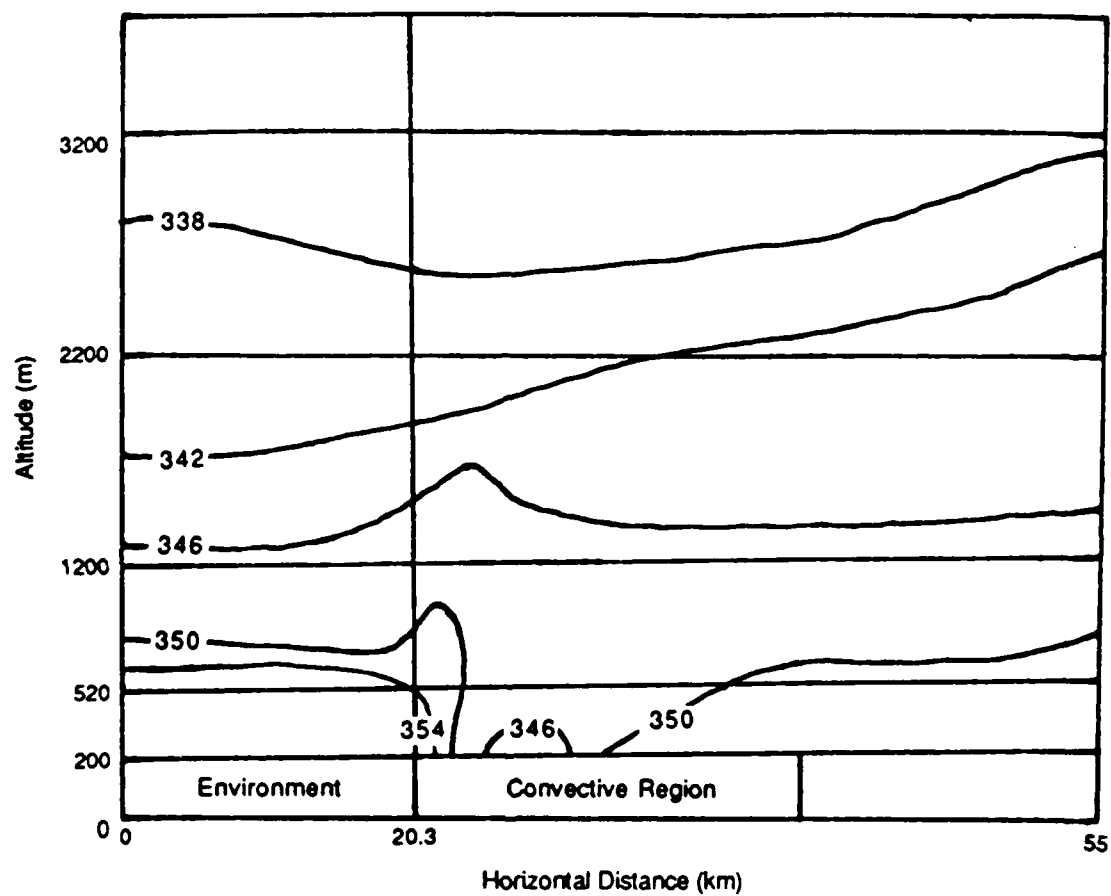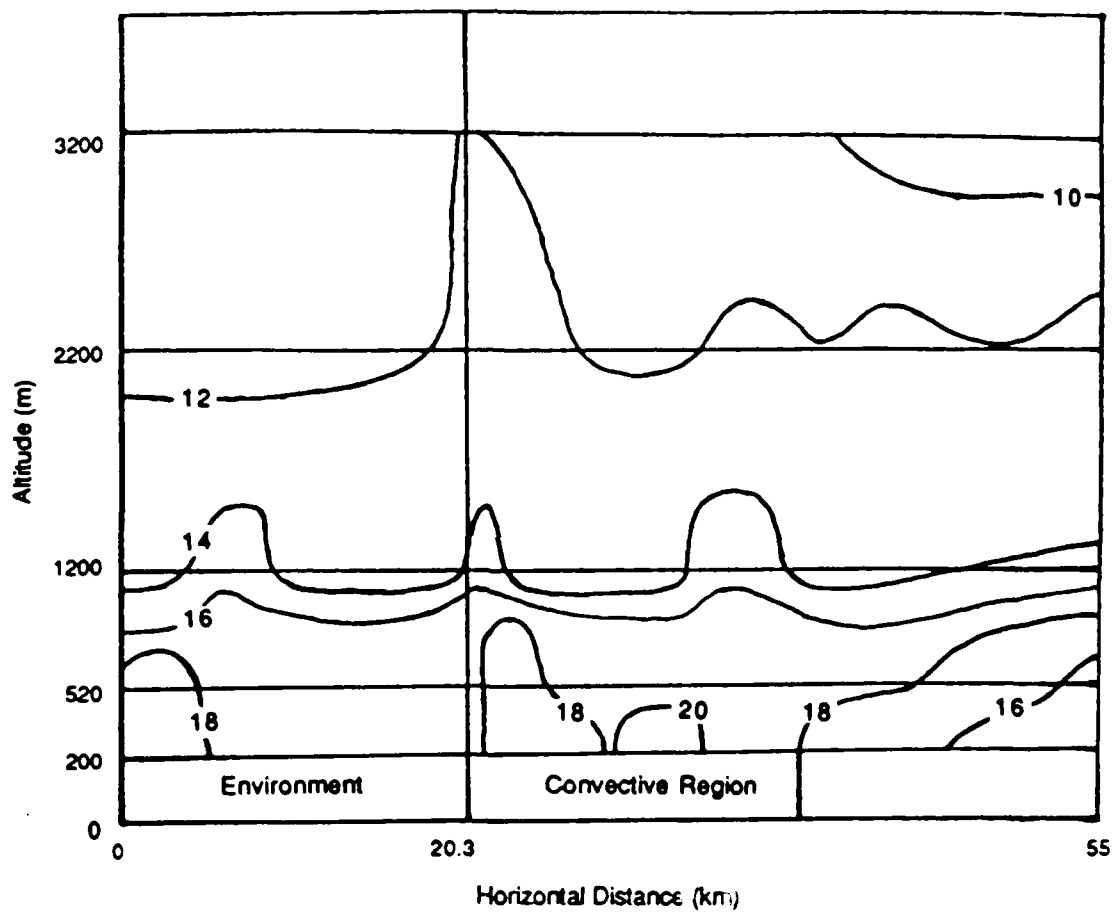
Figure 31: Composite of W (gkg⁻¹) for the EMEX 2 convective line from 200m to 3200 m. The leading edge of the convective line is at 20.3 km.

4.4 Convective Outflow

Most convective lines produce a gust front that propagates into the environment. These gust fronts enhance convergence in the environment, and in the cases where they propagate ahead of the convective line often produce a new convective line. However, based on video, thermodynamic, kinematic and inertial navigation data the gust fronts associated with the EMEX 2 lines do not appear to have propagated away from the convective lines. The gust front was defined by looking for a wind shift and for an equivalent potential temperature drop. Figure 29 shows the composite cross section of equivalent potential temperature. Because the gust front did not propagate relative to the convective region, the low equivalent potential temperature air did not spread out ahead of the leading edge of the convection. The lack of gust front movement relative to the convection is further supported by radar data, which indicates that the individual lines moved very slowly, and by calculations of the gravity current speed appropriate for the observed gust front characteristics. This gravity current speed was approximately 4.5 ms^{-1}. Comparing the gravity current speed to the environmental v_n the gravity current would not be allowed to propagate away from the convective line. The gravity current speed was calculated assuming a constant of proportionality of 0.77 (Wakimoto, 1982).

The outflow in the lower boundary layer to the rear of the convective line was also restricted by environmental flow. The low equivalent potential temperature air at 200 m only spread to 5.5 km behind the leading edge. At the boundary of this low-level outflow, a convergence zone existed. This convergence produced a secondary area of enhanced cumulus behind the main convective line. These cumulus were embedded in the precipitation of the convective line.

4.5 Tangential Jet

Figure 32 shows the composite cross section of tangential velocity (v_t). The composite cross section indicates the existence of a v_t jet at 520 m which is still defined at 1200 m. This jet has a composited maximum of 9 ms^{-1} at 520 m. The tangential jet is located on the back edge of the primary downdraft region and is approximately 9 km behind the leading edge of the convective line. The v_t jet seems to be a repeatable feature as a v_t jet was observed with both lines 1 and 2. If the v_t jet was a result of vertical mixing, the momentum would have had to have been mixed down from the 250 mb level or above (fig. 20). However, the equivalent potential temperature of the air at the level of the v_t jet would suggest that the air originated in the environment boundary layer. Thus, vertical momentum mixing can be ruled out as the cause of the jet, and it appears that the origin of the composited v_t jet must be associated with the 950 mb cyclonic circulation or eddy which was mentioned in chapter 2.

The remainder of this section will examine three hypothesis for the formation of this eddy and concentration of the circulation into the observed jet. First, it could be hypothesized that the eddy was created by the simple fluid dynamic principal related to two dimensional flow around a flat plate where the convective line is the flat plate and the sea surface and inversion bound the flow. This is not the solution as the given air flow and convective line orientation would result in an eddy that would be anticyclonic in nature contrary to the observed rotation.

The other two possibilities would be increased cyclonic flow resulting from the tilting of horizontal vorticity into the vertical or stretching of vertical vorticity. The change in vorticity given by these two terms was diagnosed by using the vorticity tendency equation. The initial vorticity in this case would be contributed by horizontal and vertical shear, and convergence contributed by the monsoon trough along which the EMEX 2 convective line formed. The tilting of horizontal vorticity can be ruled out as the cause of the eddy because the vorticity tendency
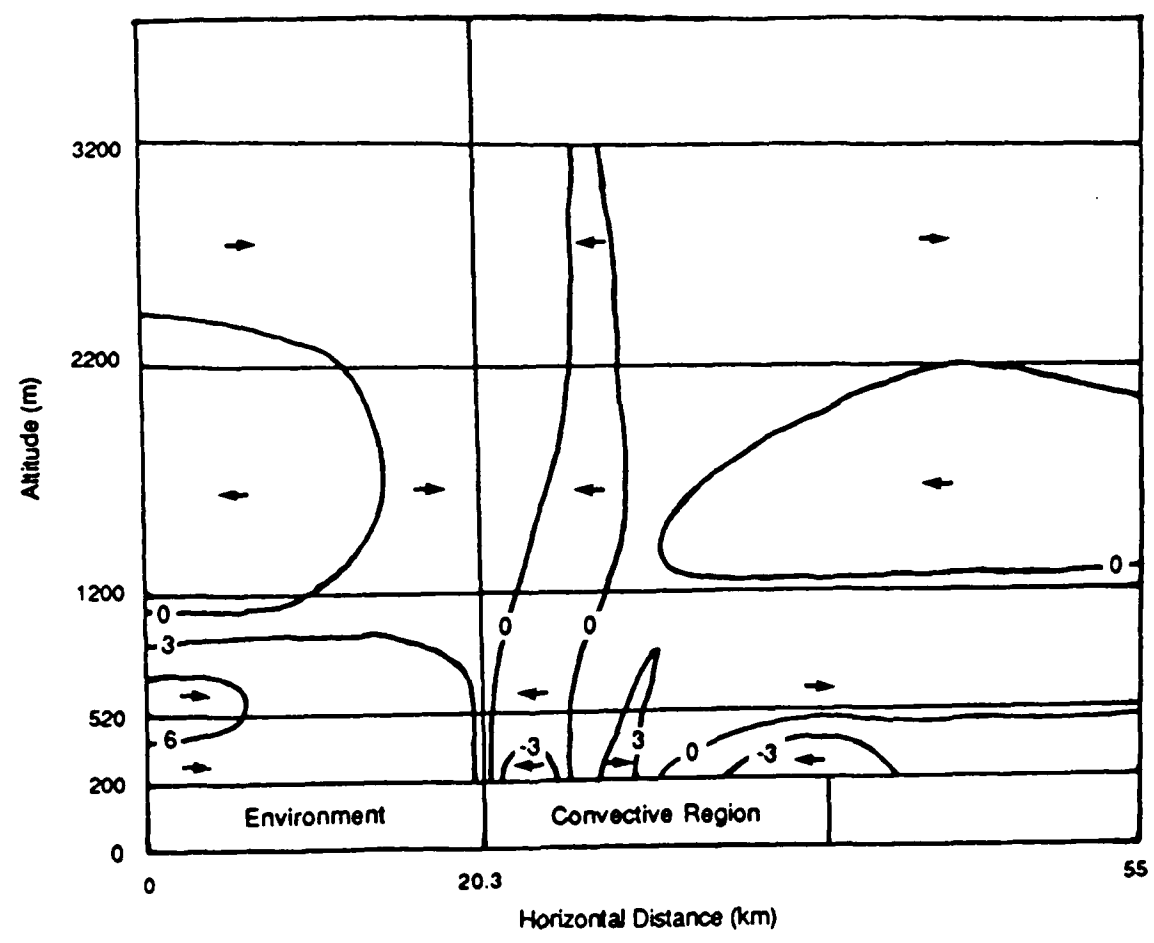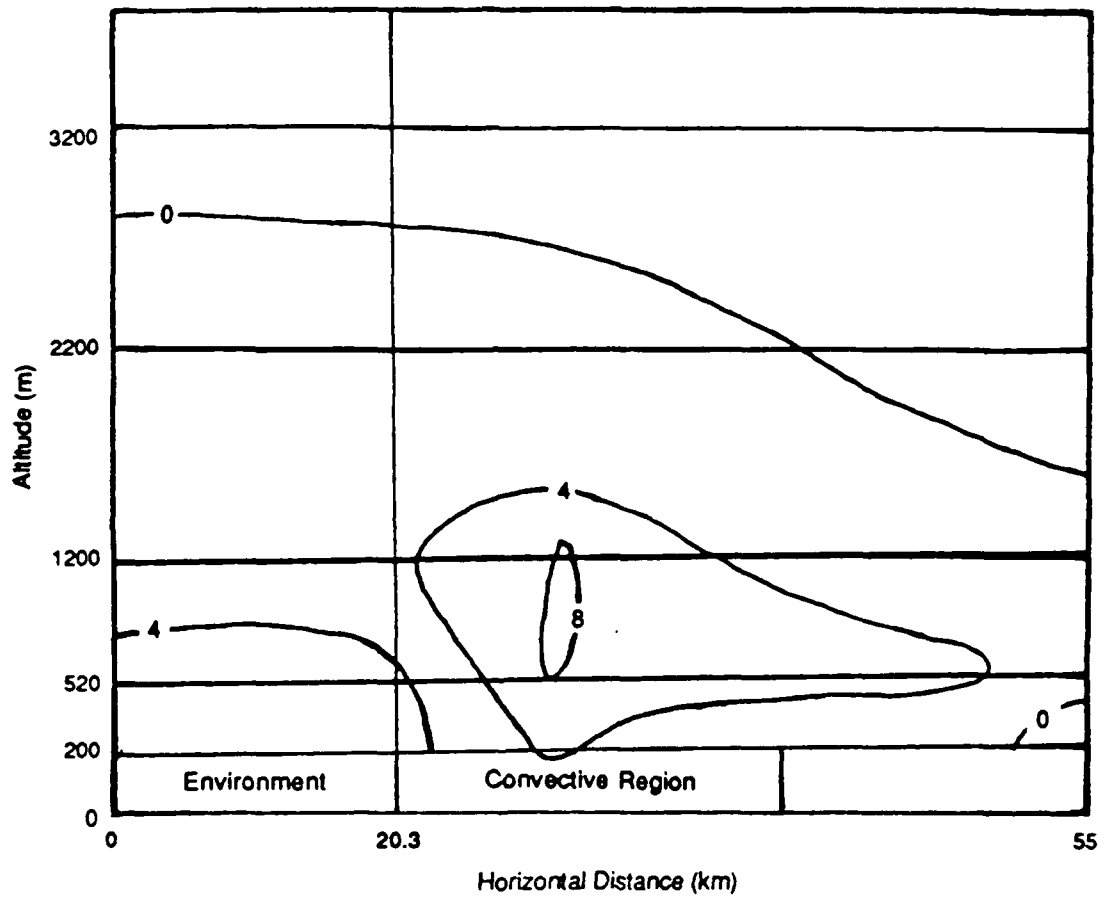
Figure 32: Composite of v_t (ms^{-1}) for the FMEX 2 convective line from 200 m to 3200 m. The leading edge of the convective line is at 20.3 km. Positive v_t is into the paper.

resulting from the tilting term would lead to anticyclonic vorticity tendency of approximately -2×10^{-7} s^{-2} at the top of the boundary layer. Because of the strong convergence across the monsoon trough, the stretching term gives a numerically reasonable result for the vertical vorticity of the eddy of approximately 2×10^{-8} s^{-2}. Thus, the stretching of the vertical vorticity of the monsoon trough is the hypothesized reason for the eddy. Because most of the convergence in the monsoon trough is focused in the convective line, the resulting vorticity is also concentrated there resulting in the jet in the region. Figure 33 show what is hypothesized as the initial mean state of v_t, and figure 34 is the observed state of v_t after the convection associated with the convective line started.

From figure 34, the perturbation component of v_t is seen to be greatest at the interfaces between the primary updraft and the primary downdraft, and between the primary downdraft and secondary updraft. Because of the spin-up (in the updraft) and the spin-down (in the downdraft) of vorticity given by the stretching term, perturbation of the tangential velocity component would be negative between the primary updraft and primary downdraft, and positive between the primary downdraft and secondary updraft. With the addition of this perturbation, v_t would be less than the mean v_t between the primary updraft and downdraft, and greater than the mean v_t between the primary downdraft and the secondary updraft. This relationship is observed at 520 meters, thus the stretching of vertical vorticity associated with the monsoon trough gives a reasonable explanation of the strength of the eddy and the v_t jet.

4.6   Secondary Updrafts in the Wake Region

This section will examine the 3 areas of secondary updrafts which were analyzed in the composited cross section of w. Low equivalent potential temperature air spreading out to the rear of the convective line produced an area of convergence approximately 9 km behind the leading
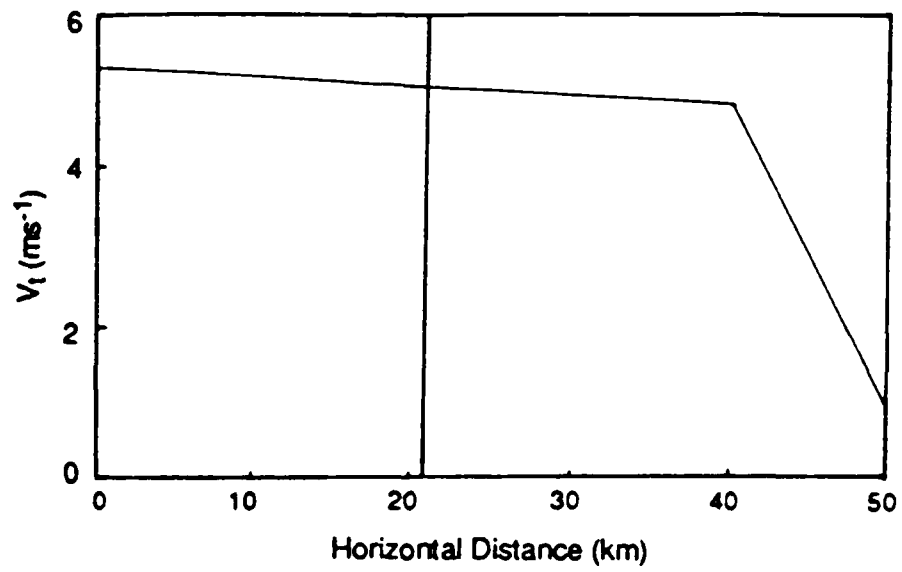
Figure 33: The hypothesized initial mean state of v_t at 520 m. The leading edge is at 20.3 km.
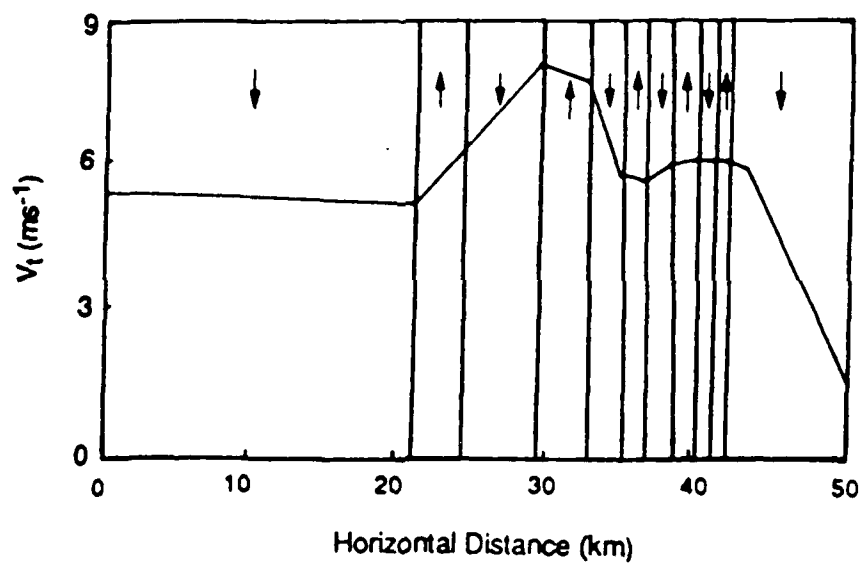
Figure 34: The observed state of v_t at 520 m. Arrows show vertical motion. The leading edge is at 20.3 km.

edge. This area of convergence caused the first secondary updraft which was embedded in the rain from the main convection. The other two secondary updrafts were farther behind the leading edge. These updrafts were associated with speed convergence in the low level flow and buoyant air with virtual temperatures greater than 29°C. The second updraft was 15 km behind the leading edge and was embedded in the precipitation of the main convective region. The third updraft was 17.7 km behind the leading edge and was evident on the video recordings of the convective line as a line of cumulus congestus. The secondary convection was stronger to the north and weaker to the south of the EMEX 2 flight legs as seen from the Electra's side camera's video recordings of the storm.

4.7   The Conceptual Model

Figure 35 is the conceptual model of the EMEX 2 type of convective line which is a composite of lines 1 and 2. The model is a two dimensional view of the convective line with the x-axis perpendicular to the major axis of the convective line.

In the environment, there was no well defined vertical motion except in the boundary layer within a few kilometers ahead of the leading edge. The convective region displays a mixing of air with origins at a number of different levels and locations. The high equivalent potential temperature downdraft air had its origins in the lower environmental boundary layer. The low equivalent potential temperature downdraft air had two possible origins. The low equivalent potential temperature air could have resulted from environmental air from near 2200 m which was ingested into the updraft then moved into the downdraft and descended to 200 m without mixing or from the mixing of environmental boundary layer air with environmental air from various levels at or above 2200 m. The updraft air had two origins. One portion had its origin in the warm moist low level environment. Secondly, because the gust front created by the convective
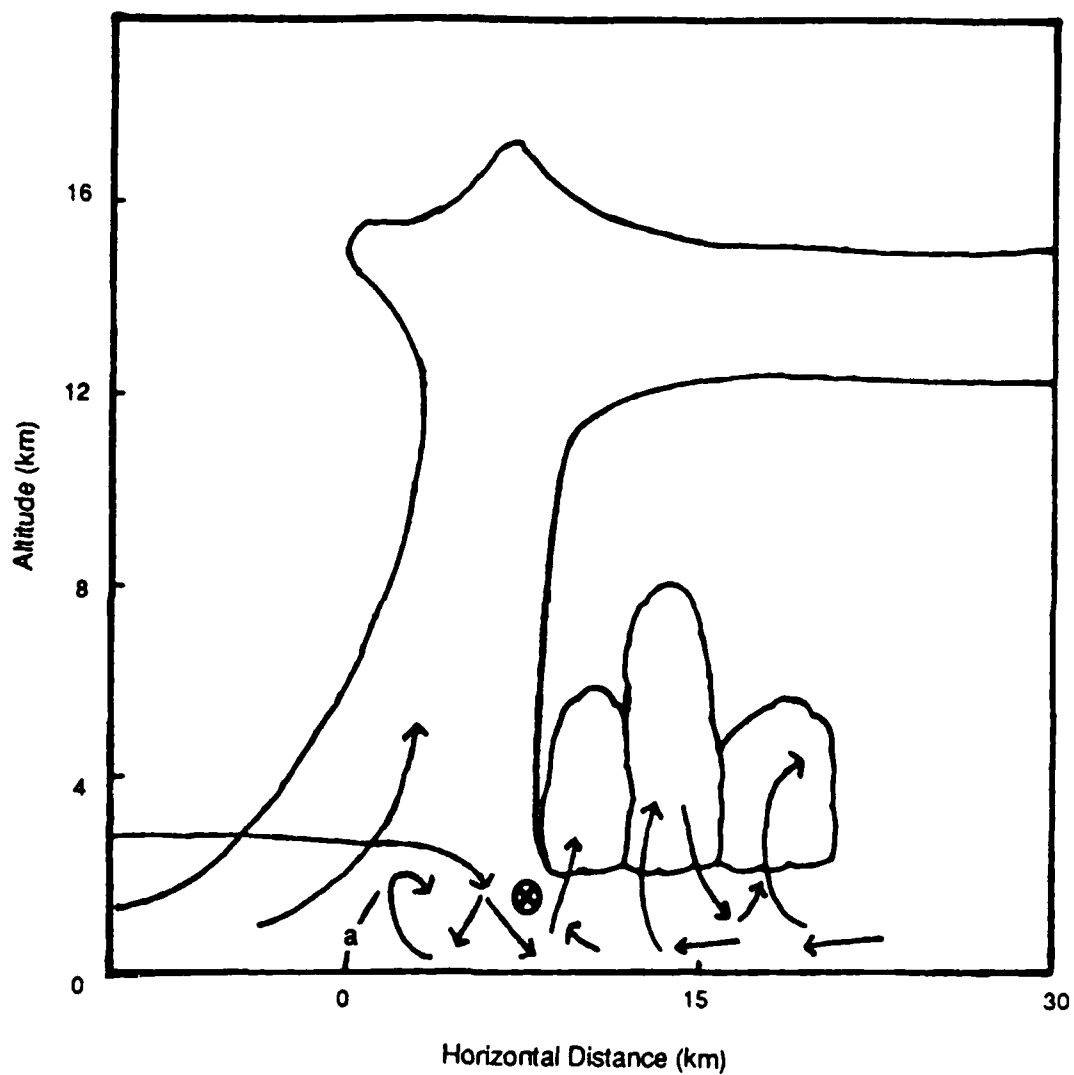
Figure 35: A two dimensional conceptual model of the EMEX 2 convective line. The arrows represent the two dimensional motion interpreted from the composites of v_n and w. The leading edge is located at (a).

downdraft never propagated ahead of the leading edge, the low equivalent potential temperature air associated with the gust front was recycled into the lower levels of the updraft.

In the rear of the convective region, there were three areas of secondary updrafts. These updrafts were caused by mesoscale low level convergence. The first two areas were embedded in the precipitation from the convective line. The third was visible on the videos of the EMEX 2 convective line. Also, located within the convective region was a tangential jet. The v_t jet was strongest at 520 m and was associated with an eddy located behind the convective line. The most notable feature of the wake region, as discussed in the previous chapters, was the lack of nimbostratus anvil.

Chapter 5

EMEX 2 BOUNDARY LAYER

The purpose of chapter 5 is to examine the turbulence structure of the environmental and wake boundary layers as a means of studying the impact of the EMEX 2 convective line on the boundary layer. Eddy correlation statistics and bulk aerodynamic surface fluxes will be used to study the boundary layer recovery in the wake region and to diagnose the dynamics of the environmental convective boundary layer.

5.1 Bulk Aerodynamic Surface Fluxes

The review of the bulk aerodynamic surface fluxes will focus on the low equivalent potential temperature wake immediately behind the convective region and on the environmental boundary layer.

5.1.1 Procedures for Calculation Of Bulk Aerodynamic Surface Fluxes

This method of calculating the sensible and latent heat fluxes at the sea surface uses only data available from the Electra aircraft flying within the boundary layer. In situ sensors provided kinematic (gust probe/inertial navigation system combination) and thermodynamic (Rosemont type 102 thermometer, thermoelectric dewpoint hygrometer) values at flight level. The temperature and wind sensors had rapid response (20 Hz) while the dewpoint was a slower response (1 Hz). A downward looking radiometer (Barnes PRT-5) was used to determine the sea surface temperature. The data from the aircraft is averaged over 4 km intervals equivalent to approximately 30 seconds of flight time. The bulk aerodynamic method used is from Smith (1980).

The first step in the algorithm was to input the aircraft altitude, sea surface temperature and dew point at flight level. Next, neutral stability was temporarily assumed, and the algorithm established an initial guess of u*, the friction velocity. Then u at 10 m was computed using the log wind law. The neutral drag coefficient appropriate for 10 m is calculated from u at 10 meters by using Smith's (1980) formula. Once this drag coefficient was calculated, it was used along with the log wind law to calculate a roughness length. The drag coefficient for flight level was also calculated using the log wind law. The next step in the algorithm was to establish the coefficient of heat transfer by using the roughness length for heat transfer and the log wind law. After the coefficient of heat transfer was established, the algorithm computes a potential temperature difference between the sea surface and flight level and the change in specific humidity (q) between flight level and the saturated value of q at the surface. The algorithm then used the coefficients of heat and moisture transfer and the drag coefficient to estimate the surface fluxes of buoyancy and momentum which were then used to estimate the Obukhov length (L).

With the initial parameters established, iterations were performed to get an accurate estimate of the ratio of flight level to Obukhov length. Then the algorithm used this ratio to estimate the surface fluxes. Using the estimated surface fluxes, the algorithm next calculated better estimates of the ratio of the flight level to the Obukhov length. This iteration was accomplished 10 times, more than enough for adequate convergence. The next step was to use the drag and heat coefficients, and a diabatic wind and temperature profile to compute u*, T*, and q* (Smith,1980). The same diabatic profile function was used for both heat and moisture. The final step in the algorithm was to use u*, T*, and q* to compute surface fluxes of latent and sensible heat.

5.1.2 Results from Bulk Aerodynamic Surface Fluxes

Table 2 shows the values of surface sensible heat flux, surface latent heat flux, surface temperature flux (T flux), surface moisture flux (q flux), and surface virtual temperature flux (T_v

Table 2: Bulk aerodynamic surface fluxes computed from data collected at 200 m.

	Environment	Environment	Wake
Sensible heat flux (Wm^{-2})	2.51	1.76	6.56
Latent heat flux (Wm^{-2})	115.16	112.52	90.12
T flux $(^{\circ}\text{Cms}^{-1})$	0.00209	0.00146	0.00546
q flux $(\text{gkg}^{-1}\text{ms}^{-1})$	0.046	0.045	0.036
T_v flux $(^{\circ}\text{Cms}^{-1})$	0.01050	0.00969	0.01204

flux) for the environment and low equivalent potential temperature wake computed from flight level data collected at 200 m. The T flux is just the sensible heat flux divided by the specific heat at constant pressure, and the q flux is the latent heat flux divided by the latent heat of evaporation. There were values for each flux computed for two flight legs in the environment and one flight leg in the wake. These fluxes are likely to have a small degree of error as a result of the high sampling altitude of approximately 200 m. This relatively high flight level could lead to an underestimate of the surface layer lapse rate of temperature and an overestimate of the surface layer lapse rate of moisture resulting in an underestimate of the T flux and an overestimate of the q flux. The other source of errors is any mixed layer shear not being accounted for properly. The recovery times of the EMEX 2 wake discussed in this section were obtained by determining the average difference between the environment and the wake profiles of T, q, or T$_v$ from the surface to 600 m then multiplying this difference by 600 m. This product was then divided by the appropriate flux to arrive at a recovery time.

The surface sensible heat flux values calculate for the environment were 2.5 Wm^{-2} and 1.7 Wm^{-2}, and for the wake it was 6.5 Wm^{-2}. Thus, the convective line had the effect of increasing the surface sensible heat flux in the disturbed boundary layer. The surface sensible heat flux was on the order of 1.6 to 2.8 times greater in the wake region than in the environment because of a decrease in surface air temperature across the convective line. The surface sensible heat fluxes for EMEX 2 and the change in the surface sensible heat flux caused by the EMEX 2 convective line are much less than the ones described by Johnson and Nicholls (1983) for their GATE convective line. Johnson and Nicholls (1983) showed surface sensible heat fluxes in the wake region to a distance of approximately 100 km behind the leading edge increased by a factor of 5 over undisturbed values. This large difference between the two systems is the result of differences in the changes to the boundary layer produced by the two convective systems. The convective line studied by Johnson and Nicholls (1983) was a fast-moving line and produced a 4°C decrease in

surface temperature between the environment and wake region, whereas the decrease caused by the EMEX 2 convective line was only 1°C. Their convective line was also characterized by 10 ms^{-1} to 15 ms^{-1} wind speeds in the wake region; much greater than the 5 ms^{-1} wind speeds characteristic of the EMEX 2 wake.

The two surface temperature flux values for the EMEX 2 environment were 0.00146°Cms^{-1} and 0.00209°Cms^{-1}. These figures correspond well with the temperature fluxes for GATE undisturbed convective boundary layers presented by Nicholls and LeMone (1980). The T flux for the wake region was 0.00546°Cms^{-1} which is a 161% to 273% increase over the environmental values. The T flux in the wake region of the GATE case studied by Johnson and Nicholls (1983) was approximately 0.0410°Cms^{-1}. With the observed T flux and the temperature change between the environmental and the wake boundary layer, the wake boundary layer would recover to the depth of the environmental boundary layer in approximately 10 hours.

The surface latent heat flux in the environment of the EMEX 2 convective line was 115 Wm^{-2} which is comparable to the values found by Johnson and Nicholls (1983) for their GATE case. However, the 90 Wm^{-2} surface latent heat flux in the EMEX 2 wake was much less than the wake values found by Johnson and Nicholls (1983). The surface latent heat flux for the EMEX 2 wake was approximately 80% of the environmental value. This is a significant difference from the factor of 4 increase in surface latent heat flux in the wake region found by Johnson and Nicholls (1983). The large increase in surface latent heat flux in the GATE wake was the result of a large decrease in q across the convective line and the 10 ms^{-1} to 15 ms^{-1} wind in the wake. The decrease in the surface latent heat flux across the EMEX 2 convective line is attributed to the relatively small 9% decrease in q and the 34% decrease in wind speed across the convective line.

The q flux for the EMEX 2 environment was 0.045 gkg^{-1}ms^{-1} which corresponds well with the q fluxes for GATE convective boundary layers presented by Nicholls and LeMone (1980). In the EMEX 2 wake, the q flux was somewhat lower with a value of 0.036 gkg^{-1}ms^{-1} or 80% of the

environmental value. This q flux would result in a recovery time of less than 10 hours for q for a 600 meter deep boundary layer in the wake.

The most vital turbulent flux for the forcing of convective boundary layer turbulence is the T_v flux. For the EMEX 2 case, the T_v flux for the environment was $0.0101°Cms^{-1}$ compared to $0.0120°Cms^{-1}$ for the wake. Thus, T_v flux for the wake was 19% greater than for the environment because the large increase in T flux in the wake over compensated for the decrease in q flux.

The fact that the T flux compensated for a decrease in the q flux in the wake is shown by the ratio of T flux and q flux contributions to the T_v flux. In the environment, the T flux contribution was only 21% as large as the q flux contribution while in the wake the T flux contribution was 83% of the q flux contribution. Thus, convective turbulence in the environmental convective boundary layer was driven mainly by the q flux, whereas the q flux and T flux both contributed significantly to forcing convective turbulence in the wake boundary layer. With the above T_v flux, the wake would have recovered into a convective boundary layer of 600 meters in approximately 10 hours. The equivalent potential temperature recovery throughout a 600 meter deep boundary layer is dictated by the the recovery of q and T, thus the equivalent potential temperature recovery in the wake region can be no faster than 10 hours with only surface fluxes. However, the wake boundary layer can recover faster if the fluxes of T and q from above the inversion into the boundary layer are considered. From eddy correlation turbulence statistics which are presented in Section 5.2, there was warm dry air transferred across the inversion via entrainment. This process was not considered in detail, but this entrainment of warm dry air could decrease the wake boundary layer recovery time.

The recovery time on the order of 10 hours is on the upper end of the range of typical wake recovery times of 2-10 hours during GATE (Johnson and Nicholls, 1983). However, for general circulation models it is not only the wake recovery time which is significant, but also the horizontal extent of the wake and the development of convection in the disturbed region are also important.

Convection can occur in the wake region before the boundary layer recovers to its undisturbed height. The convection operating in a disturbed region has less net energy transfer per unit mass than convection in an undisturbed region (Barnes and Garstang, 1982). The abundance of this convection makes it important to the overall energy budget of the tropics.

The EMEX 2 wake was small in horizontal extent because of the quasi-stationary line propagation. Thus, the recovery time of the wake is misleading. The area 50 km behind the EMEX 2 leading edge could support convection well before the wake produced by the EMEX 2 convective line recovered. Thus, the horizontal extent of wake which is a characteristic of convective line type is significant to its parameterization in general circulation models.

5.2 Eddy Correlation Turbulence Statistics

The review of eddy correlation fluxes will focus on the wake region and the convective boundary layer of the environment.

5.2.1 Procedures for Calculation of Eddy Correlation Turbulence Statistics

The program used to calculate the eddy correlation fluxes was designed to read 20 Hz "in situ" data for a given time interval of data collection at a constant altitude. The turbulence statistics were computed for flight legs 13 km to 25 km long having horizontally homogeneous turbulence. The program first calulated the mean and standard deviation of each variable. Any data point with a value greater than three standard deviations away from the mean for that variable was replaced by the preceding data point unless the data point was the first data point in the time interval. In the latter case, it was replaced by the mean value for the given time interval. The next step was to subject the data to a subprogram which removed any linear trends. After the linear trends were removed, the data was in perturbation form and ready to be used to calculate the various eddy correlation statistics.

5.2.2 Results from Eddy Correlation Turbulence Statistics

The eddy correlation turbulence statistics are used in this section to determine the cause of the turbulence in the environmental boundary layer. The turbulence structure of the wake will also be discussed. The turbulence statistics presented in tables 3 and 4 will be used to examine the turbulence characteristics of these two regions. There were two flight legs of data analyzed at an altitude of 200 m for the environment, and only one flight leg of data was analyzed for the other areas presented in the tables.

In the environmental boundary layer, an upward surface flux of T_v was determined in Section 5.1.2. with the q flux contribution dominating over the T flux contribution. Thus, there was a significant surface evaporation component to the turbulence forcing along with a lesser surface temperature flux forcing. With the given bulk aerodynamic surface fluxes, buoyancy is responsible for some if not all of the turbulence in the environmental boundary layer. The vertical velocity skewness observations are as expected for a convective boundary layer with an inversion height near 600 m (Young, 1988). Furthermore, the ratios of vertical velocity variance to the two components of horizontal variance are greater than 1.0 as expected in a convective boundary layer (Young, 1988). Thus, a wide variety of turbulence information suggests that the environmental boundary layer is convective. However, the 1.36 value of the ratio of w variance to w* in the EMEX 2 environmental convective boundary layer is much larger than it could be in a purely convective boundary layer (Young,1988); hence, shear must be a significant contributor to the turbulence forcing. w* was shown to be the appropriate scaling parameter for boundary layer convection by Deardorff (1970).

Deardorff (1972) showed the ratio of inversion height to the Obukhov length was an important stability parameter describing the relative contribution of shear and buoyancy forcing. LeMone (1973) studied three cases where atmospheric rolls existed when this ratio was approximately equal to 10. She concluded that shear was a major source of energy for these rolls

Table 3: Eddy correlation turbulence statistics at 200 m for the two environment flight legs and at 180 m for the wake flight leg.

	Environment	Environment	Wake
$\overline{W'^2}$ (m^2s^{-2})	0.353	0.323	0.058
$\overline{U'^2}$ (m^2s^{-2})	0.221	0.161	0.633
$\overline{V'^2}$ (m^2s^{-2})	0.185	0.258	0.648
$\overline{W'^3}$ (m^3s^{-3})	0.149	0.113	0.004
$\overline{T'^2}$ $(^\circ C^2)$	0.101	0.003	0.057
$\overline{W'T'}$ $(^\circ Cms^{-1})$	-0.013	0.003	-0.004

Table 4: Eddy correlation turbulent statistics at 530 m for the environment and at 516 m for the wake.

	Environment	Wake
$\overline{W'^2}$ (m^2s^{-2})	0.299	0.065
$\overline{U'^2}$ (m^2s^{-2})	0.441	0.135
$\overline{V'^2}$ (m^2s^{-2})	0.298	0.090
$\overline{W'^3}$ (m^3s^{-3})	0.255	0.004
$\overline{T'^2}$ $(^\circ C^2)$	0.026	0.015
$\overline{W'T'}$ $(^\circ Cms^{-1})$	-0.044	-0.004

via the inflection point mechanism. From the surface fluxes of the EMEX 2 system, the ratio of the inversion height to the Obukhov length was approximately equal to 10. Thus, the environmental boundary layer for EMEX 2 meets this criteria for the support of atmospheric rolls with the energy for these rolls coming from environmental shear. These atmospheric rolls would enable the turbulence to be stronger than would be possible with only the observed convective forcing. Some suggestion of these rolls was visible in the alignment of boundary layer cumulus ahead of the EMEX 2 convective line.

The vertical velocity variance dropped significantly in the wake compared with the environmental convective boundary layer at the two low altitude flight levels, 180 m and 520 m. This decrease in turbulence intensity was not the result of a decrease in buoyant forcing because, as shown in section 5.1.2, the T_v flux increased by 19% in the wake compared with the environmental convective boundary layer. Thus, something other than a decrease in buoyant forcing suppressed the convection in the wake. The origins of this suppression are explained below using other turbulence statistics.

In the wake region, the value of temperature variance at 180 m is greater than the value at 520 m (Table 4). This profile can be compared with that in the environmental region where temperature variance decreases downward from near the 600 m inversion to the lowest flight level at 200 m. The environmental profile is typical of those observed within the convective boundary layer while the wake profile is similar to those observed within and above a capping inversion (Young, 1988). These similarities would suggest that the inversion height in the wake was approximately 200 m. From 180 m to 520 m, the wake lapse rate was 60% of the dry adiabatic lapse rate resulting in a stable layer. This stable layer between 180 m and 520 m corroborates the occurrence of a low inversion height in the wake region. The downward shift of the inversion resulted in a shift of the lowest flight level from approximately 1/3 the inversion height to approximately the inversion height itself and hence the observed decrease in the variance of w.

Further evidence of the stability of the air at 180 m and 500 m in the wake region comes from the ratio of the horizontal components of velocity variance to the vertical component. The variance of u and v are greater than the variance of w as is typical in the capping inversion (Young,1988). The turbulent statistics suggest that 180 m was within the boundary layer but the stability near the inversion might have led to the potential temperature at 180 m being an overestimate of the potential temperature in the boundary layer. This overestimate would have caused an underestimate of the air/sea temperature difference and thus, an underestimate of the bulk aerodynamic surface temperature fluxes.

From the surface buoyancy fluxes it can be concluded that below the inversion there was a convective boundary layer. This shallow recovering wake boundary layer could not be thoroughly sampled because of flight safety restrictions, so the use of all other available information was essential to our understanding. In the recovering wake, the ratio of inversion height to the Obukhov length was approximately 70. This suggests that the recovering boundary layer was characterized by three dimensional thermals rather than two dimensional rolls.

Chapter 6

CONCLUSIONS

The EMEX 2 convective line was an extreme case of a convectively dominated system. It appears to warrant the addition of another class of convective line to the Barnes and Sieckman (1984) classification scheme. This new class would be a quasi-stationary convective line class with line speed near zero and limited nimbostratus production.

On 15 January 1987, lines 1 and 2 never produced the extensive nimbostratus anvil characteristic of previously studied tropical convective lines. The convection associated with these lines progressed into the mature stage of the Leary and Houze (1979) classification scheme, but it never produced the extensive nimbostratus anvil characteristic of the mature stage. The nimbostratus anvils of lines 1 and 2 were nearly an order of magnitude smaller than the nimbostratus anvils observed during GATE. The ability of a convective line to produce nimbostratus anvil is a function of horizontal moisture advection from the convective region into the mesoscale stratiform anvil region. Furthermore, the advection of moisture from the convective region into the mesoscale stratiform anvil region is a function of convective line speed and of the environmental shear profile of v_n.

As the case was in GATE, the environmental thermodynamic factors did not control the velocity of the EMEX 2 convective line. The line speed was related to the cross line shear. As the cross line shear increases, the line speed increases as shown by this study and by the study of Barnes and Sieckman (1984). Also of significance is the along line shear. As the along line shear increases the line speed is seen to decrease.

The low line speed and low cross line shear environment produced short lived convective cells along the EMEX 2 convective line. These convective cells rained heavily into their own updrafts or into adjacent convective updrafts. The net effect was the existence within the wake region of a

significant amount of air with origins in the environmental convective boundary layer as opposed to the predominately mid-level origins of air in the wakes of faster lines. Hence, there were small equivalent potential temperature and W drops across the EMEX 2 convective line. This result supports the GATE findings of Barnes and Sieckman (1984). They found decreasing across line differences in thermodynamic variables with decreasing line speed. The net result of decreasing line speed is to have a systematic decrease in the CAPE difference between the environment and the wake as the line speed decreases.

The EMEX 2 convective line decreased the depth of the convective boundary layer but not as drastically as the faster GATE lines. Furthermore, it had minimal effect on the q flux, as the wake value was 80% of the environmental value. The T flux was changed by nearly the same percentage, but it increased in the wake region by 19% over the environmental value. The T flux and q flux accounted for a wake recovery time on the order of 10 hours, which is comparable to previously published recovery times. However, a more important feature in this case is the limited horizontal extent of the wake region. The undisturbed area 50 km behind the EMEX 2 leading edge could support convection well before the wake produced by the convective line recovered.

The use of eddy correlation information can provide insight into the boundary layer forcing and turbulence structure in tropical convective systems. This information could be very useful for verifying boundary layer aspects of the mesoscale models which provide much of the understanding of tropical convective lines.

Based on previous observational studies, Brown (1979) and Johnson and Young (1983) suggested that the diabatic heating profile for a typical convective system is composed of two components, one associated with the convective component of the system and the other with the stratiform component. The variation of the ratio of these two components is crucial to climate modelers. The EMEX 2 system provides evidence that a very wide range of values is possible for this ratio. Because the region of nimbostratus anvil associated with the EMEX 2 system was far

less extensive than with previously studied convective lines, the diabatic heating profile would be dominated by the convective component.

To parameterize the ratio of the convective and stratiform components of the convective heating, one must assess the extent of the stratiform precipitation associated with a convective line. Thus, the diabatic heating parameterization of general circulation models could be improved by incorporating the relationship between line speed and horizontal extent of nimbostratus anvil.

To accomplish this improved parameterization, one would need to parameterize line speed from environmental shear and line orientation. From this study and from GATE results the line speed can be related to the environmental shear; however, the line orientation was not discussed and is worthy of further study.

BIBLIOGRAPHY

Barnes, G. M., and K. Sieckman, 1984: The environment of fast- and slow-moving tropical mesoscale convective cloud lines. Mon. Wea. Rev., 112, 1782-1794.

Betts, A. K., R. W. Grover and M. W. Moncrieff, 1976: Structure and motion of tropical squall lines over Venezuela. Quart. J. Roy. Meteor. Soc., 102, 395-404.

Bolton, D., 1980: The computation of equivalent potential temperature. Mon. Wea. Rev., 108, 1046-1053.

Brown, J. M., 1979: Mesoscale unsaturated downdrafts driven by rainfall evaporation: A numerical study. J. Atmos. Sci., 36, 313-338.

Businger, J. A., 1973: Turbulent transfer in the atmospheric surface layer. Workshop on Micrometeorology, D. A. Haugen, Ed., AMS, 67-100.

Byers, H. R., and R. R. Braham, Jr., 1949: The thunderstorm. U. S. Government Printing Office, Washington, D. C., 287 pp.

Chong, M., P. Amayenc, G Scialom, and J. Testud, 1987: A tropical squall line observed during the COPT 81 experiment in West Africa. Part I: Kinematic structure inferred from dual-doppler radar data. Mon. Wea. Rev., 115, 670-694.

Cohen, C. and W. M. Frank, 1987: Simulation of tropical convective systems. Part I: A cumulus parameterization. J. Atmos. Sci., 44, 3787-3820.

Deardorff, J. W., 1970: Convective velocity and temperature scales for the unstable planetary boundary layer and for Rayleigh convection. J. Atmos. Sci., 27, 1211-1213.

Deardorff, J. W., 1972: Numerical investigation of neutral and unstable planetary boundary layers. J. Atmos. Sci., 29, 91-115.

Frank, W. M., 1978: The life cycles of GATE convective systems. J. Atmos. Sci., 35, 1256-1264.

Fujita, T. T., 1955: Results of detailed synoptic studies of squall lines. Tellus, 7, 405-436.

Gamache, J. F., F. D. Marks and R. W. Burpee, 1987: The equatorial mesoscale experiment. Hurricane Research Division, 1987.

Gamache, J. F. and R. A. Houze, Jr, 1982: Mesoscale air motions associated with tropical squall line. J. Atmos. Sci., 110, 118-135.

Garstang, M., 1967: Sensible and latent exchange in low latitude synoptic scale systems. Tellus, 19, 492-508.

Hamilton, R. A., and J. W. Archbold, 1945: Meteorology of Nigeria and adjacent territory. Quart. J. Roy. Meteo. Soc., 71, 231-262.

Hartmann, D. L., H. H. Hendon and R. A. Houze, Jr., 1984: Some implications of the mesoscale circulations in tropical cloud clusters for large-scale dynamics and climate. J. Atmos. Sci., 41, 113-121.

Hauser, D., F. Roux and P. Amayenc, 1988: Comparison of two methods for the retrieval of thermodynamic and microphysical variables from doppler radar measurements: Application to the case of a tropical squall line. J. Atmos. Sci., 45, 1285-1303.

Houze, R. A., Jr., 1977: Structure and dynamics of a tropical squall-line system. Mon. Wea. Rev., 105, 1540-1567.

Houze, R. A., Jr., 1982: Cloud clusters and large-scale vertical motions in the tropics. J. Meteor. Soc. Japan, 60, 396-410.

Houze, R. A., Jr. and E. N. Rappaport, 1984: Air motions and precipitation structure of an early summer squall line over the eastern tropical Atlantic. J. Atmos. Sci., 41, 553-574.

Johnson, R. H., and M. E. Nicholls, 1983: A composite analysis of the boundary layer accompanying a tropical squall line. Mon. Wea. Rev., 111, 308-319.

Johnson, R. H., and G. S. Young, 1983: Heat and moisture budgets of tropical mesoscale anvil clouds. J. Atmos. Sci., 40, 2138-2147.

Keenan, T. D., and S. C. Martin, 1987: AMEX radar atlas. Volume II: AMEX phase II. BMRC Research Report No. 9., Bureau of Meteorology Research Centre, GPO. Box 1289K, Melbourne, Australia 3001.

Kruger, S. K., 1988: Numerical simulation of tropical cumulus clouds and their interaction with the sub-cloud layer. J. Atmos. Sci., 45, 2221-2250.

Leary, C. A., and R. A. Houze, Jr., 1979: The structure and evolution of convection in a tropical cloud cluster. J. Atmos. Sci., 36, 437-457.

LeMone, M. A., 1973: The structure and dynamics of horizontal roll vortices in the planetary boundary layer. J. Atmos. Sci., 30, 1077-1091.

LeMone, M. A., 1976: Modulation of turbulence energy by longitudinal rolls in an unstable planetary boundary layer. J. Atmos. Sci., 33, 1308-1320.

LeMone, M. A., and E. J. Zipser, 1980: Cumulonimbus vertical velocity events in GATE. Part I: Diameter, intensity, and mass flux. J. Atmos. Sci., 37, 2444-2457.

Moncrieff, M. W., and M. J. Miller, 1976: The dynamics and simulations of tropical cumulonimbus and squall lines. Quart. J. Roy. Meteo. Soc., 102, 373-394.

Newton, C. W., 1950: Structure and mechanisms of the prefrontal squall line. J. Meteor., 7, 210-222.

Nicholls, S., and M. A. LeMone, 1980: The fair weather boundary layer in GATE: The relationship of subcloud fluxes and structure to the distribution and enhancement of cumulus clouds. J. Atmos. Sci., 37, 2035-2050.

Ogura, Y., and M. T. Liou, 1980: The structure of a midlatitude squall line: A case study. J. Atmos. Sci., 37, 553-567.

Pedgley, D. E., 1962: A mesosynoptic analysis of the thunderstorms on 28 August 1958. Brit. Meteor. Office, Geophys. Memo., No. 106, 74 pp.

Roux, F., J. Testud, M. Payen and B. Pinty, 1984: West African squall-line thermodynamic structure retrieved from dual-doppler radar observations. J. Atmos. Sci., 41, 3104-3121.

Smith, S. D., 1980: Wind stress and heat flux over the ocean in gale force winds. J. P. O., 10, 709-725.

Smithsonian Institution, 1966: Smithsonian Meteorological Tables, Washington D. C., 295-301.

Smull, B. F., and R. A. Houze, Jr., 1985: A midlatitude squall line with a trailing region of stratiform rain: Radar and satellite observations. Mon. Wea. Rev., 113, 117-133.

Smull, B. F., and R. A. Houze, Jr., 1987: Dual-Doppler radar analysis of a midlatitude squall line with a trailing region of stratiform rain. J. Atmos. Sci., 44, 2128-2148.

Szoke E. J., and E. J. Zipser, 1986: A radar study of convective cells in mesoscale systems in GATE. Part II: Life cycles of convective cells. J. Atmos. Sci., 43, 199-218.

Wakimoto R. M., 1982: The life cycle of thunderstorm gusts fronts as viewed with doppler radar and rawinsonde data. Mon. Wea. Rev., 110, 1060-1082.

Zipser, E. J., 1969: The role of organized unsaturated convective J. Appl. Meteor., 8, 799-814.

Zipser, E. J., 1977: Mesoscale and convective-scale downdrafts as distinct components of squall-line circulation. Mon. Wea. Rev., 105, 1568-1589.

Zipser, E. J., R. J. Meitan and M. A. LeMone, 1981: Mesoscale motion fields associated with a slowly moving GATE convective band. J. Atmos. Sci., 38, 1725-1750.